The Discrete Cones Method in Two-Dimensional Neutron Transport Computation

Y. Watanabe and C.W. Maynard

May 1984

UWFDM-574

FUSION TECHNOLOGY INSTITUTE

UNIVERSITY OF WISCONSIN

MADISON WISCONSIN

The Discrete Cones Method in Two-Dimensional Neutron Transport Computation

Y. Watanabe and C.W. Maynard

Fusion Technology Institute
University of Wisconsin
1500 Engineering Drive
Madison, WI 53706

http://fti.neep.wisc.edu

May 1984

UWFDM-574

THE DISCRETE CONES METHOD IN TWO-DIMENSIONAL NEUTRON TRANSPORT COMPUTATION

Y. Watanabe and C.W. Maynard

Fusion Engineering Program
Nuclear Engineering Department
University of Wisconsin-Madison
Madison, Wisconsin 53706

May 1984

UWFDM-574

TABLE OF CONTENTS

1. INTRODUCTION

Many neutronics analyses of fusion reactors have been carried out by 1-D or 2-D discrete ordinates codes (S_N codes) such as ANISN,[1] ONEDANT,[2], DOT,[3] TWOTRAN,[4] and TRIDENT-CTR.[5]

Although a one-dimensional geometry cannot model actual reactors, 1-D calculations have been routinely performed. Because 1-D calculations are relatively inexpensive, they are used when many similar calculations are required. One of the examples is a calculation to optimize physical lengths and material compositions of blanket and shield.

To lessen the geometrical error, 2-D S_N codes are sometimes used. 2-D codes can model the poloidal cross section of a toroidal device quite well. Furthermore, partitioning the whole reactor system into components, each subsystem can be modeled by 2-D geometry. Therefore, 2-D S_N codes are very useful tools to obtain better geometrical modeling, when rigorous 3-D analyses by a Monte Carlo code do not afford.

However, the 2-D S_N method has a serious problem for the systems that people in the fusion neutronics field are analyzing. It has long been recognized that an anomaly, the so-called ray effect, exists in a solution of a highly absorbing material and a void.[6] Many methods have been proposed to fix it for a solution in a non-void. Emergence of detailed fusion reactor designs reminded us of the importance of the ray effect in a void, which we shall call the ray streaming effect. Since a fusion reactor system includes localized neutron sources in a vacuum and has many narrow ducts such as neutral beam injectors, microwave launchers, and vacuum pump inlets, the ray streaming effect is particularly important in the fusion neutronics. To overcome the anomaly, people in this field have been developing several hybrid

methods utilizing the S_N solution and the other solution. One of them is to use a Monte Carlo method in a void and the S_N method in a non-void.[7] While this method eliminates the ray streaming effect, it is not efficient. As is well known, good spatial and angle resolutions by a Monte Carlo calculation are not obtained as easily as with a S_N solution. On the other hand, a S_N solution requires spatial and angle distributions of particle sources by the Monte Carlo calculation. Therefore, coupling the two methods requires much effort. Another method is to use an analytical formula of the first-flight kernel to obtain fluxes produced by a source in a void.[8] The fluxes are used as surface sources for the following S_N calculation. This method is much more efficient than the former, but neglecting the contribution of collided particles makes a large error for some problems.

Seed and Maynard proposed another hybrid method,[9-11] in which a deterministic method for a vacuum streaming calculation is utilized in a S_N code. Their method was formulated only for x-y geometry. Later, Clark developed a similar method for r-z geometry, the so-called streaming matrix hybrid method.[12,13] His method was successfuly implemented in the TRIDENT-CTR program.[14] Their basic idea is that since the ray effect is caused by tracing particles in discrete directions, tracing particles so that no direction is missed eliminates the anomaly.

In the present report, we choose Maynard's approach[11] and construct a theory of the so-called discrete cones method. In this method, a direction space is partitioned into cones and particles in a cone are simultaneously traced. Outgoing and incoming fluxes and a source in a spatial mesh cell are related by transfer and escape matrices.

The general theory will be described in Section 2. In Section 3, the method will be applied to a solution in a void for x-y geometry. Two different schemes will be formulated. In one scheme, a void is partitioned into mesh cells, and the transfer and escape matrices will be derived for a mesh cell. In another scheme, boundary surfaces of a void are partitioned into subsurfaces and the transfer matrix between fluxes on the subsurfaces will be derived. The schemes will be implemented in S_N programs to solve several sample problems. Section 4 will conclude this report.

References for Section 1

1. W.W. Engle, Jr., "A User's Manual for ANISN, A One-Dimensional Discrete Ordinates Code with Anisotropic Scattering," Oak Ridge Gaseous Diffusion Plant, K-1693 (1967).

2. R.D. O'Dell et al., "User's Manual for ONEDANT: A Code Package for One-Dimensional, Diffusion-Accelerated, Neutral-Particle Transport," Los Alamos National Laboratory, LA-9184-M (1982).

3. W.A. Rhoades, D.B. Simpson, R.L. Childs and W.W. Engle, Jr., "The DOT-IV Two-Dimensional Discrete Ordinates Transport Code with Space-Dependent Mesh and Quadrature," Oak Ridge National Laboratory, ORNL-TM-6529 (1979).

4. K.D. Lathrop and F.W. Brinkley, "TWOTRAN-II: An Interfaced, Exportable Version of the TWOTRAN Code for Two-Dimensional Transport," Los Alamos Scientific Laboratory, LA-4848-MS (1973).

5. T.J. Seed, "TRIDENT-CTR User's Manual," Los Alamos Scientific Laboratory, LA-7835-M (1979).

6. K.D. Lathrop, "Ray Effects in Discrete Ordinates Equations," Nucl. Sci. Eng. 32, 357-369 (1968).

7. W.T. Urban, T.J. Seed and D.J. Dudziak, "Engineering Test Facility Vacuum Pumping Duct Shield Analysis," Nucl. Tech./Fusion 2, 261-271 (1982).

8. R.A. Lille, R.T. Santoro, R.G. Alsmiller, Jr. and J.M. Barns, "Neutron and Gamma Ray Streaming Calculations for the Engineering Test Facility Neutral Beam Injectors," Nucl. Tech./Fusion 2, 325-333 (1982).

9. T.J. Seed, "Deterministic Streaming," Los Alamos Scientific Laboratory, LA-7911-PR, 32-32 (1979).

10. C.W. Maynard and T.J. Seed, "Deterministic Streaming," Los Alamos Scientific Laboratory, LA-8135-PR, 33-44 (1979).

11. C.W. Maynard, "Integral Transport in Void Regions for Discrete Ordinates," Los Alamos Scientific Laboratory, LA-8771-PR, 53-63 (1981).

12. B.A. Clark, "The Development and Application of the Discrete Ordinates-Transfer Matrix Hybrid Method for Deterministic Streaming Calculations," Los Alamos National Laboratory, LA-9357-T (1982).

13. B.A. Clark, "The Streaming Matrix Hybrid Method for Discrete Ordinates Calculations," Proc. Top. Mtg. ANS Mathematics and Computation Division, Salt Lake City, UT, March 28-31, 1983.

14. B.A. Clark, W.T. Urban and D.J. Dudziak, "Evaluation of the Streaming Matrix Method for Discrete Ordinates Duct Streaming Calculations," Proc. Sixth Int. Conf. on Radiation Shielding, Tokyo, May 16-20, 1983.

2. GENERAL THEORY OF THE DISCRETE CONES METHOD

2.1 The Discrete Ordinates Approximation

A numerical solution of the transport equation requires an approximation of the direction vector $\underline{\Omega}$. In the discrete ordinates approximation, a set of discrete directions is selected. The set is selected so that numerical integrations of a function with respect to the direction vector should be optimal in terms of accuracy because most quantities of interest and the scattering source term in the transport equation are represented as integrals of some weight function times the angular flux over the unit sphere of directions.

Many sets of discrete directions have been constructed. However, we restrict our discussion to the symmetric equal weight quadrature set EQ_N[1] since we shall use this set when both the discrete ordinates method and the discrete cones method are applied in one program, or the discrete cones method is applied in the whole domain of a problem.

We define the direction vector $\underline{\Omega}$ in terms of polar coordinates as illustrated in Fig. 2.1(a), in which $\mu = \sqrt{1 - \xi^2} \cos \chi$ and $\eta = \sqrt{1 - \xi^2} \sin \chi$. This coordinate system is used in X-Y geometry. In R-Z geometry, a coordinate system shown in Fig. 2.1(b) is used. Unless anything is mentioned, all the following discussion in this chapter will be made in the X-Y coordinate system. We assume the symmetry of the direction space about $\mu - \eta$, $\eta - \xi$, and $\xi - \mu$ planes. Then, the following integral over an octant of the unit sphere of directions is evaluated:

$$I = \int f(\Omega)\, d\Omega = \int_0^1 \int_0^{\pi/2} f(\xi,\chi)\, d\xi d\chi \,. \tag{2.1}$$

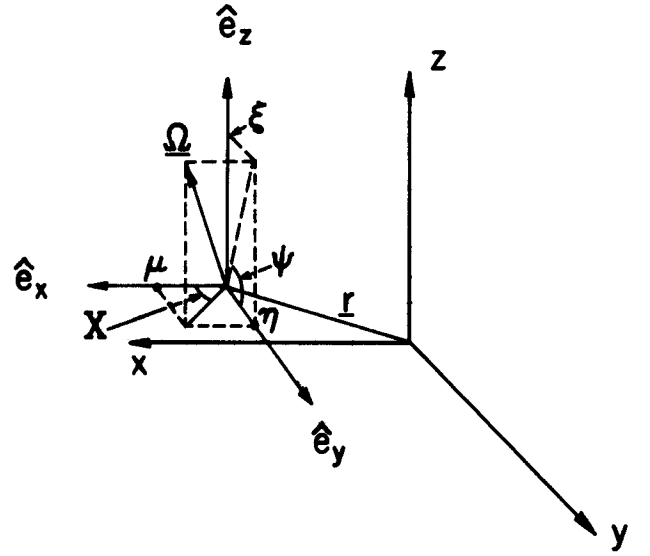

Fig. 2.1(a) The coordinate system for X-Y geometry.

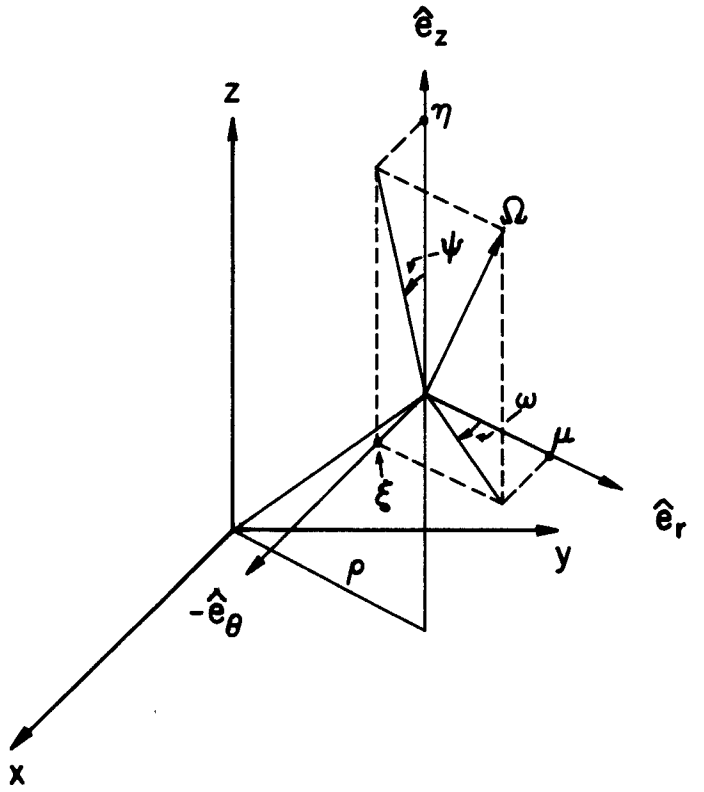

Fig. 2.1(b) The coordinate system for R-Z geometry.

In the discrete ordinates approximation, this integral is approximated by

$$I_{DO} = 2\pi \sum_{m=1}^{M} w_m f(\xi_m, \chi_m) \tag{2.2}$$

where w_m is the weight factor, (μ_m, η_m, ξ_m) is a point on the unit sphere of directions, $\chi_m = \arctan(\eta_m/\mu_m)$, M is the number of points in the octant, and μ_m, η_m, ξ_m, and w_m satisfy $\mu_m^2 + \eta_m^2 + \xi_m^2 = 1$ and $\sum_{m=1}^{M} w_m = 1/4$.

For the EQ_N quadrature set, we assume equal weights; that is, $w_m = 1/(4M)$. The points are determined by solving the following equation (2.3), which states the approximation (2.2) is exact for polynomials $P(\mu,\xi) = \mu^k \xi^\ell$, where $k + \ell \leq N$, k and ℓ are positive even integers or zeros.

$$2\pi \sum_{m=1}^{M} w_m \mu_m^k \xi_m^\ell = \int_0^1 d\xi \int_0^{\pi/2} d\chi \; \mu^k \xi^\ell \; . \tag{2.3}$$

Equation (2.3) gives $N(N + 2)/8$ equations. Meanwhile, there are $N(N + 2)/4$ unknowns when $M = N(N + 2)/8$. Hence, imposing further assumptions of symmetry on the quadrature points and reducing the number of unknowns, we can solve a set of nonlinear equations (2.3) to find the quadrature set.

2.2 The Discrete Cones

In the discrete cones approximation, the unit sphere of directions is divided into cones, $\Delta\Omega_m$, where $\Delta\Omega_m = [\chi_{m-1/2}, \chi_{m+1/2}] \times [\xi_{m-1/2}, \xi_{m+1/2}]$. We make four assumptions to determine boundaries of the cones on the spherical surface:

1. The direction space is symmetrical with respect to $\mu - \eta$, $\eta - \xi$, and $\xi - \mu$ planes; consequently, only one octant of the unit sphere will be considered.

2. The areas of the cones, $\Delta\Omega_m$, are equal for all m on the octant; i.e.,

$$\iint_{\Delta\Omega_m} d\underline{\Omega} = \iint_{\Delta\Omega_n} d\underline{\Omega} \qquad \text{for all m and n such that } m \neq n. \tag{2.4}$$

3. The ξ-direction is divided by N/2 ξ-planes (i.e., ξ = constant) for the DC_N approximation.

Meanwhile, for the i'th ξ-level, the domain of the variable χ: $[0,\pi/2]$, is divided equally into N/2 - i + 1 intervals, where i = 1 and N/2 corresponds to the lowest and highest ξ-levels, respectively. As a result of this assumption, there are N(N + 2)/8 cones in an octant, which is the same as the number of the discrete directions in the discrete ordinates approximation. This assumption also imposes rotational symmetry about the ξ-axis in the direction space. The use of constant ξ-levels is made in order to make analytical integrations of the transfer matrix elements easier. It is noted that the quadrature points of the EQ_N set reside nearly at the center of the cones. This is illustrated in Fig. 2.2.

Under the above assumptions, we shall find the cone boundaries. First, the second assumption leads to

$$\iint_{\Delta\Omega_m} d\underline{\Omega} = \frac{\pi/2}{N(N+2)/8} = \frac{4\pi}{N(N+2)} \tag{2.5}$$

because $\iint_{\text{an octant}} d\underline{\Omega} = \pi/2$ and there are N(N + 2)/8 (= M) cones in the octant. Performing the integration of the left most side results in

$$\int_{\xi_{m-1/2}}^{\xi_{m+1/2}} d\xi \int_{\chi_{m-1/2}}^{\chi_{m+1/2}} d\chi = (\xi_{m+1/2} - \xi_{m-1/2})(\chi_{m+1/2} - \chi_{m-1/2}) \,. \tag{2.6}$$

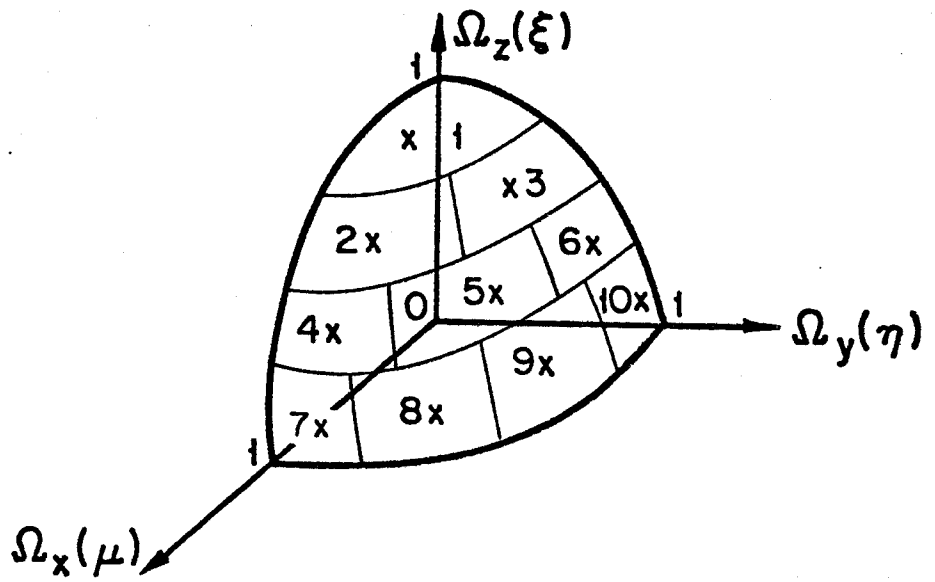

Fig. 2.2 Schematic diagram of cones in the DC_8 approximation for X-Y geometry.

Next, if we consider the i'th ξ-level, the third assumption leads to

$$\chi_{m+1/2} - \chi_{m-1/2} = \frac{\pi/2}{N/2 - i + 1} . \tag{2.7}$$

Thus, by Eqs. (2.6) and (2.7),

$$\xi_{m+1/2} - \xi_{m-1/2} = \frac{4(N - 2i + 2)}{N(N + 2)} . \tag{2.8}$$

For the first ξ-level, Eq. (2.8) becomes $\xi_{3/2} - \xi_{1/2} = 4/(N + 2)$. Since $\xi_{1/2} = 0$, $\xi_{3/2} = 4/(N + 2)$. As long as the cone resides in the first ξ-level, $\xi_{m-1/2} = 0$ and $\xi_{m+1/2} = 4/(N + 2)$. For the second ξ-level, $\xi_{m+1/2}$ is obtained by Eq. (2.8) from the known $\xi_{m-1/2}$. Also, $\chi_{m+1/2}$ ($m = 1, 2, \ldots, M$) are easily found.

The cone boundaries for the DC_8 approximation used in this work are listed in Tables 2.1 and 2.2 for X-Y and R-Z geometries, respectively.

Having determined the cones, the integral is approximated in the discrete cones approximation as follows:

$$I_{DC} = 2\pi \sum_{m=1}^{M} \left(\iint_{\Delta\Omega_m} d\underline{\Omega} \right) f(\xi_m, \chi_m) = 2\pi \sum_{m=1}^{M} \hat{w}_m f(\xi_m, \chi_m) \tag{2.9}$$

where $\hat{w}_m = 2/(N(N + 2))$, $\xi_m \simeq \frac{1}{2} (\xi_{m+1/2} + \xi_{m-1/2})$, $\chi_m \simeq \frac{1}{2} (\chi_{m+1/2} + \chi_{m-1/2})$, and (ξ_m, χ_m) is a quadrature point of the EQ_N set. The approximation (2.9) is called the double triangle rule (DTR) because of its similarity to the triangle rule for one-dimensional numerical integration. This is the same as Eq. (2.2) when the EQ_N set is used; hence, Eq. (2.9) is exact for polynomials such as $\mu^k \xi^\ell$ where $k + \ell \leq N$, and k and ℓ are positive even integers or zeros.

Table 2.1. Cone Boundaries for the DC_8 Approximation in X-Y Geometry

ξ-Level	m	χ_+	χ_-	ξ_+	ξ_-
1	10	1.5708E+00	1.1781E+00	4.0000E-01	0.0000E+00
1	9	1.1781E+000	7.8540E-01	4.0000E-01	0.0000E+00
1	8	7.8540E-01	3.9270E-01	4.0000E-01	0.0000E+00
1	7	3.927E-01	0.0000E+00	4.0000E-01	0.0000E+00
2	6	1.5708E+00	1.0472E+00	7.0000E-01	4.0000E-01
2	5	1.0472E+00	5.2360E-01	7.0000E-01	4.0000E-01
2	4	5.2360E-01	0.0000E+00	7.0000E-01	4.0000E-01
3	3	1.5708E+00	7.8540E-01	9.0000E-01	7.0000E-01
3	2	7.8540E-01	0.0000E+00	9.0000E-01	7.0000E-01
4	1	1.5708E+00	0.0000E+00	1.0000E+00	9.0000E-01

Table 2.2. Cone Boundaries for the DC_8 Approximation in R-Z Geometry

η-Level	m	ω_+	ω_-	η_+	η_-
1	1	1.5708E+00	0.0000E+00	1.0000E+00	9.0000E-01
2	2	7.8540E-01	0.0000E+00	9.0000E-01	7.0000E-01
2	3	1.5708E+00	7.8540E-01	9.0000E-01	7.0000E-01
3	4	5.2360E01	0.0000E+00	7.0000E-01	4.0000E-01
3	5	1.0472E+00	5.2360E-01	7.0000E-01	4.0000E-01
3	6	1.5708E+00	1.0472E+00	7.0000E-01	4.0000E-01
4	7	3.9270E-01	0.0000E+00	4.0000E-01	0.0000E+00
4	8	7.8540E-01	3.9270E-01	4.0000E-01	0.0000E+00
4	9	1.1781E+00	7.8540E-01	4.0000E-01	0.0000E+00
4	10	1.5708E+00	1.1781E+00	4.0000E-01	0.0000E+00

However, when the current, which is another important quantity in transport theory, is evaluated, the DTR differs from the approximation used by the discrete ordinates method. The current J_+ is defined by

$$J_+ = \iint_{\underline{\Omega}\cdot\underline{n}>0} f(\underline{\Omega})\underline{\Omega}\cdot\underline{n}\ d\underline{\Omega} \tag{2.10}$$

where J_+ is equivalent to the number of particles crossing a surface with unit area per unit time, and $\underline{n}$ is a vector outward-normal to the surface.

In the discrete ordinates approximation, J_+ is given by

$$J_{DO} = 2\pi \sum_{m=1}^{MT} \mu_m w_m f(\underline{\Omega}_m) \tag{2.11}$$

where we define $\mu = \underline{\Omega}\cdot\underline{n}$ and MT is the number of discrete directions satisfying $\mu_m > 0$. In the discrete cones approximation, J_+ is given by

$$J_{DC} = \sum_{m=1}^{MT} \left(\iint_{\Delta\Omega_m} \underline{\Omega}\cdot\underline{n}\ d\underline{\Omega}\right) f(\underline{\Omega}_m) \tag{2.12}$$

where $\underline{\Omega}_m$ is a quadrature point of the EQ_N set.

2.3 Numerical Solutions of the Transport Equation by the Discrete Cones Approximation

In this work, we are concerned with a solution of the time independent neutron transport equation:

$$\underline{\Omega}\cdot\nabla\Psi(\underline{r},\underline{\Omega},E) + \sigma_t(\underline{r},E)\ \Psi(\underline{r},\underline{\Omega},E) = S(\underline{r},\underline{\Omega},E) \tag{2.13}$$

where $\Psi(\underline{r},\underline{\Omega},E)$ is the angular flux at a spatial point $\underline{r}$ in the direction $\underline{\Omega}$ for energy E, $\sigma_t(\underline{r},E)$ is the total macroscopic cross section, and $S(\underline{r},\underline{\Omega},E)$ is the source term. Furthermore, the source term is divided into three terms: the scattering term S_c, the fission source term S_f, and the external source term $Q(\underline{r},\underline{\Omega},E)$. The explicit formulas for S_c and S_f are as follows:

$$S_c(\underline{r},\underline{\Omega},E) = \int_0^\infty dE' \iint_{4\pi} d\underline{\Omega}\ \sigma_s(\underline{r};\underline{\Omega}'\to\underline{\Omega},E'\to E)\ \Psi(\underline{r},\underline{\Omega}',E') \tag{2.14}$$

$$S_f(\underline{r},E) = \frac{1}{4\pi}\int_0^\infty \nu(\underline{r},E'\to E) \iint_{4\pi} \sigma_f(\underline{r},E')\ \Psi(\underline{r},\underline{\Omega}',E')\ d\Omega'dE' \tag{2.15}$$

where σ_s is the differential scattering cross section, ν is the spectrum of fission neutrons, and σ_f is the fission cross section.

We apply the multigroup method to the energy variable of Eq. (2.13) to obtain the following transport equation for the g'th energy group:[2]

$$\underline{\Omega}\cdot\nabla\Psi_g(\underline{r},\underline{\Omega}) + \sigma_{tg}(\underline{r})\ \Psi_g(\underline{r},\underline{\Omega}) = S_g(\underline{r},\underline{\Omega}) \tag{2.16}$$

where $$S_g(\underline{r},\underline{\Omega}) = S_{cg}(\underline{r},\underline{\Omega}) + S_{fg}(\underline{r}) + Q_g(\underline{r},\underline{\Omega})$$

$$S_{cg}(\underline{r},\underline{\Omega}) = \sum_{h=1}^{G} \iint_{4\pi} d\underline{\Omega}'\ \sigma_{sh\to g}(\underline{r};\underline{\Omega}'\to\underline{\Omega})\ \Psi_h(\underline{r},\underline{\Omega}') \tag{2.17}$$

and $$S_{fg}(\underline{r}) = \frac{1}{4\pi}\sum_{h=1}^{G} \nu_{h\to g}(\underline{r})\ \sigma_f(\underline{r})\ \phi_g(\underline{r})\ . \tag{2.18}$$

The scalar flux $\phi_g(\underline{r})$ is defined by

$$\phi_g(\underline{r}) = \iint_{4\pi} d\Omega\ \Psi_g(\underline{r},\underline{\Omega})\ . \tag{2.19}$$

Since we use the standard multigroup method and we are interested in solving the neutron transport equation for an energy group, in the remainder of this paper we shall omit the subscript g.

To solve the neutron transport equation numerically, in the discrete ordinates method the finite difference equations are derived from Eq. (2.16). On the other hand, in the discrete cones method we solve the integral form of the transport equation:[3]

$$\Psi(\underline{r},\underline{\Omega}) = \int_0^{S_o} ds\, S(\underline{r}',\underline{\Omega}) e^{-\alpha(\underline{r}',\underline{r})} + \Psi(\underline{r}_s,\underline{\Omega}) e^{-\alpha(\underline{r}_s,\underline{r})} \tag{2.20}$$

where $s = |\underline{r} - \underline{r}'|$, $\underline{r}' = \underline{r} - s\underline{\Omega}$, $\underline{r}_s = \underline{r} - s_o\underline{\Omega}$, and $\alpha(\underline{r}',\underline{r})$ is the optical path length defined by

$$\alpha(r',r) = \int_0^{|\underline{r}-\underline{r}'|} ds\, \sigma_t\left(\underline{r} - \frac{s(\underline{r} - \underline{r}')}{|\underline{r} - \underline{r}'|}\right) . \tag{2.21}$$

In a void, Eq. (2.20) becomes

$$\Psi(\underline{r},\underline{\Omega}) = \int_0^{S_o} ds\, Q(\underline{r}',\underline{\Omega}) + \Psi(\underline{r}_s,\underline{\Omega}) . \tag{2.22}$$

To solve Eq. (2.20) or (2.22), first we partition the spatial domain of a problem into mesh cell D_i. Regarding $\Psi(\underline{r}_s,\underline{\Omega})$ as an incoming angular flux into the mesh cell D_i, we can calculate the outgoing angular flux on the cell D_i by either Eq. (2.20) or (2.22). The equations may be solved along a characteristic line that corresponds to a discrete direction in the discrete ordinates approximation; then the method is called the characteristic method.[4] In the discrete cones method, however, characteristics in a cone are simultaneously

traced. As a result, there are no directions which are not traced. This continuity of tracing makes the new method mitigate the ray effects.

Equations (2.20) and (2.22) are multiplied by $\underline{\Omega}\cdot\underline{n}$ where $\underline{n}$ is the unit vector outward-normal to the cell boundary. Then, they are integrated over cone m and an outgoing surface to find the particle conservation equation of the m'th cone:

$$J^{+}_{i\ell m} = \sum_{k} J^{-}_{i\ell km} + q_{i\ell m} \tag{2.23}$$

where $J^{+}_{i\ell m}$ is the m'th outgoing cone current on surface ℓ of cell i, $J^{-}_{i\ell km}$ is the number of particles entering at surface k and crossing surface ℓ in cone m, and $q_{i\ell m}$ is the number of particles produced in cell i and crossing surface ℓ in cone m. The summation with respect to k is taken because particles entering several surfaces actually cross surface ℓ.

To go further, we define the cone flux Ψ_m by

$$\Psi_m(\underline{r}) = \frac{\iint_{\Delta\Omega_m} \underline{\Omega}\cdot\underline{n}\ \Psi(\underline{r},\underline{\Omega})\ d\underline{\Omega}}{\iint_{\Delta\Omega_m} \underline{\Omega}\cdot\underline{n}\ d\underline{\Omega}} . \tag{2.24}$$

As a point on the outgoing surface varies and the direction sweeps in cone m, the point and direction on the incoming surface also vary. Hence, carefully analyzing the correspondence of the spatial points and directions on the incoming and outgoing surfaces, we obtain the following recursive relation among the outgoing and incoming cone fluxes, and the source in the mesh cell:

$$\Psi_{i\ell m} = \sum_k \sum_{m'} T_{i\ell k}^{mm'} \Psi_{ikm'} + \sum_{m'} P_{i\ell}^{mm'} S_{im'} \tag{2.25}$$

where $\Psi_{i\ell m}$ is the m'th cone flux averaged over surface ℓ of cell i, $T_{i\ell k}^{mm'}$ is the ratio of particles that enter surface k in cone m' to particles that cross surface ℓ in cone m, and $P_{i\ell}^{mm'}$ is the fraction of particles that are produced in cell i in cone m' and cross surface ℓ in cone m. By particle conservation, any uncollided particle leaving cell i through surface ℓ in cone m must enter the cell on one of boundary surfaces in one of cones. Since the coefficient $T_{i\ell k}^{mm'}$ represents transport of uncollided particles, the summations over all k and m' must be unity:

$$\sum_k \sum_{m'} T_{i\ell k}^{mm'} = 1 \quad . \tag{2.26}$$

In a matrix form, Eq. (2.25) becomes

$$\underline{\Psi}_{i\ell} = \sum_k \underline{\underline{T}}_{i\ell k} \underline{\Psi}_{ik} + \underline{\underline{P}}_{i\ell} \underline{S}_i \tag{2.27}$$

and we call $\underline{\underline{T}}_{i\ell k}$ the transfer matrix and $\underline{\underline{P}}_{i\ell k}$ the escape matrix.

Boundary conditions of the discrete cones method differ from those of the discrete ordinates method in that the cone flux Ψ_m^{DC} is used instead of the angular flux in a discrete direction, Ψ_m^{DO}. Let $\underline{n}$ be a unit vector outward-normal to a boundary surface ∂D of a spatial domain D. Then, the vacuum boundary condition is given by

$$\Psi_m^{DC}(\underline{r}_s) = 0 \tag{2.28}$$

for $\underline{r}_s$ on the boundary and any cone m such that $\underline{\Omega}\cdot\underline{n} < 0$ and $\underline{\Omega}\varepsilon\Delta\Omega_m$. The reflective boundary condition is given by

$$\Psi_m^{DC}(\underline{r}_s) = \Psi_{m_r}^{DC}(\underline{r}_s) \tag{2.29}$$

where $\underline{r}_s\varepsilon\partial D$, and cone m and cone m_r are mirror images of each other about the tangential plane at $\underline{r}_s$.

When both the discrete ordinates and the discrete cones methods are applied in the same calculation, the following adjustment factors must be considered so that particles are conserved on the interface between solutions by the two methods. The particle conservation for cone m is represented by

$$\left(\iint_{\Delta\Omega_m} \underline{\Omega}\cdot\underline{n}\ d\underline{\Omega}\right)\ \Psi_m^{DC} = (\underline{\Omega}_m\cdot\underline{n})\ w_m\Psi_m^{DO}\ . \tag{2.30}$$

If the adjustment factor is defined by

$$\alpha_m = \frac{\iint_{\Delta\Omega_m} \underline{\Omega}\cdot\underline{n}\ d\underline{\Omega}}{(\underline{\Omega}_m\cdot\underline{n})\ w_m} \tag{2.31}$$

then the discrete cone flux Ψ_m^{DC} is related with the discrete ordinate flux Ψ_m^{DO} by

$$\psi_m^{DC} = \frac{1}{\alpha_m}\ \Psi_m^{DO}\ . \tag{2.32}$$

The adjustment factors of the DC_8 approximation are listed on Tables 2.3(a) and 2.3(b) for X-Y geometry and R-Z geometry, respectively.

Table 2.3(a). The Adjustment Factors for the DC_8 Approximation in X-Y Geometry

Cone No.	α_X	α_Y
1	0.9564	0.9870
2	0.9739	0.9963
3	0.9936	0.9811
4	0.9963	0.9739
5	1.0033	1.0033
6	1.0344	0.9667
7	0.9870	0.9564
8	0.9811	0.9936
9	0.9667	1.0344
10	0.9482	0.9482

Table 2.3(b). The Adjustment Factors for the DC_8 Approximation in R-Z Geometry

Cone No.	α_r	α_z
1	0.9482	0.9892
2	0.9667	0.9919
3	1.0344	0.9919
4	0.9811	0.9976
5	1.0033	0.9526
6	0.9936	0.9976
7	0.9870	1.0145
8	0.9963	0.9372
9	0.9739	0.9372
10	0.9564	1.0145

Now returning to Eq. (2.27), we describe its solution in an abstract manner. Given incoming angular fluxes on boundary surfaces of a system, Eq. (2.27) provides 2×IT×JT×MT equations for cell edge cone fluxes. Here, IT and JT are the number of spatial intervals in the two orthogonal directions of the system. MT is the total number of discrete cones, and MT = N(N + 2)/2 for the DC_N approximation. Since the source term $\underline{S}$ depends on cell average angular fluxes, there are 3×IT×JT×MT unknowns. Therefore, IT×JT×MT equations beside Eq. (2.27) must be provided. In our method, these are obtained by taking account of particle balance for a spatial mesh cell and a cone. In a void, meanwhile, Eq. (2.27) gives sufficient equations for the solution.

The 3×IT×JT×MT equations are represented in the following way by using operator notation:

$$\Psi = T\Psi + PS = T\Psi + P(C\Phi + Q) \tag{2.33}$$

and

$$\Phi = M\Psi \ . \tag{2.34}$$

Here, Ψ denotes a vector containing 2×IT×JT×MT cell edge cone fluxes, Φ denotes a vector containing IT×JT×MT cell average angular fluxes, and T and P are the transfer and escape operators, respectively. The collision operator C may be further divided into scattering and fission terms. Q is an external source. M is an operator which maps the cell edge cone flux Ψ to the cell average angular flux Φ.

Equations (2.33) and (2.34) are not solved by directly inverting the matrix, but an iterative method is used. In the multigroup method, the term $C\Phi$ includes contributions by upscattered and downscattered neutrons as well as

fission neutrons from other energy groups. Hence, the outer iteration scheme is employed by assuming the contributions from other energy groups. With this assumption, Eqs. (2.33) and (2.34) become one-group equations.

Since we sweep the spatial mesh cells in four octants of the direction space separately, and $C\Phi$ is related to the cone fluxes of all the octants, we do not know the correct scattering term until we finish sweeping in all the octants. Hence, we need another iteration process, the inner iteration. Using the unknown cell average angular fluxes by the previous inner iteration, we iterate until a convergence criterion is satisfied.

For the inner iteration, Eqs. (2.33) and (2.34) are written as

$$\Psi^{(k+1)} - T\Psi^{(k+1)} = P(C\Phi^{(k)} + Q) \tag{2.35}$$

$$\Phi^{(k+1)} = M\Psi^{(k+1)} \tag{2.36}$$

where k and k+1 indicate the k'th and k+1'th inner iteration, respectively.

The outer and inner iteration processes of the discrete cones method are the same as those of the discrete ordinates method. However, the discrete cones method employs finite difference operators for T, P, C, and M which are different from the operators used by the discrete ordinates method. Therefore, the numerical properties of the new method must be carefully examined so that the convergence and stability are confirmed.

2.4 The Accuracy of the Double Triangle Rule (DTR)

First, we shall prove the following two theorems on the convergence of the approximate integrations (2.9) and (2.12).

Theorem 2.1. Suppose I is the exact solution of the integral (2.1), and I_{DTR} is the integration by the double triangle rule (2.9). Then $\|I - I_{DTR}\|_\infty \leq \frac{C}{N}$ for any three times continuously differentiable function $f \in C^3(\Omega)$, where $\|\cdot\|_\infty = \sup|\cdot|$, C is a positive constant, N is the order of the approximation, and $N >> 1$.

Theorem 2.2. Suppose J is the exact integration of integral (2.10), and J_{DTR} is given by the approximation (2.12). Then $\|J - J_{DTR}\|_\infty \leq \frac{C}{N}$ for any $f \in C^3(\Omega)$, where C is a positive constant, N is the order of the approximation, and $N >> 1$.

Proof of Theorem 2.1. Let us define $E[f] = I - I_{DTR}$. The Taylor's formula for a n times continuously differentiable two variable function $f(\xi,\chi)$ is given by

$$f(\xi,\chi) = f(\xi_o,\chi_o) + \sum_{k=1}^{n-1} \left((\xi - \xi_o)\frac{\partial}{\partial\xi} + (\chi - \chi_o)\frac{\partial}{\partial\chi}\right)^k \frac{f(\xi_o,\chi_o)}{k!}$$

$$+ \frac{1}{n!}\left((\xi - \xi_o)\frac{\partial}{\partial\xi} + (\chi - \chi_o)\frac{\partial}{\partial\chi}\right)^n f(\xi_o + \theta(\xi - \xi_o),\ \chi_o + \theta(\chi - \chi_o))$$

where $0 < \theta < 1$. Then, E[f] becomes

$$E[f] = \sum_{m=1}^{M}\sum_{k=1}^{n-1}\frac{1}{k!}\int_{\xi_-}^{\xi_+} d\xi \int_{\chi_-}^{\chi_+} d\chi\left((\xi - \xi_m)\frac{\partial}{\partial\xi} + (\chi - \chi_m)\frac{\partial}{\partial\chi}\right)^k f(\xi_m,\chi_m) + Rn \qquad (2.37)$$

where $\xi_\pm = \xi_{m\pm1/2}$, $\chi_\pm = \chi_{m\pm1/2}$, $M = N(N+2)/8$, and $Rn = \sum_{m=1}^{M}\frac{1}{n!}\iint_{\Delta\Omega_m}\left((\xi - \xi_m)\frac{\partial}{\partial\xi} + (\chi - \chi_m)\frac{\partial}{\partial\chi}\right)^n f(\xi_m + \theta(\xi - \xi_m),\ (\chi_m + \theta(\chi - \chi_m))\, d\xi d\chi$. Here, it is assumed that $\xi_m = (\xi_{m+1/2} + \xi_{m-1/2})/2$ and $\chi_m = (\chi_{m+1/2} + \chi_{m-1/2})/2$.

The first term of the right hand side of Eq. (2.37) is integrated as follows:

$$\sum_{m=1}^{M}\sum_{k=1}^{n-1}\frac{1}{k!}\int_{\xi_-}^{\xi_+}d\xi\int_{\chi_-}^{\chi_+}d\chi\sum_{\ell=0}^{k}\binom{k}{\ell}(\xi-\xi_m)^{\ell}(\chi-\chi_m)^{k-\ell}\left(\frac{\partial}{\partial\xi}\right)^{\ell}\left(\frac{\partial}{\partial\chi}\right)^{k-\ell}f(\xi_m,\chi_m)$$

$$=\sum_{m=1}^{M}\sum_{k=1}^{n-1}\frac{1}{k!}\sum_{\ell=0}^{k}\binom{k}{\ell}\frac{2(\Delta\xi_m/2)^{\ell+1}}{\ell+1}\frac{2(\Delta\chi_m/2)^{k-\ell+1}}{k-\ell+1}\left(\frac{\partial}{\partial\xi}\right)^{\ell}\left(\frac{\partial}{\partial\chi}\right)^{k-\ell}f(\xi_m,\chi_m)$$

$$=\sum_{m=1}^{M}\sum_{k=1}^{n-1}\sum_{\ell=0}^{k}\frac{2^{-k}\Delta\xi_m^{\ell+1}\Delta\chi_m^{k-\ell+1}}{(\ell+1)!\,(k-\ell+1)!}\left(\frac{\partial}{\partial\xi}\right)^{\ell}\left(\frac{\partial}{\partial\chi}\right)^{k-\ell}f(\xi_m,\chi_m)\ ,$$

where $\Delta\xi_m=\xi_+-\xi_-$, $\Delta\chi_m=\chi_+-\chi_-$, $\binom{k}{\ell}=k!/(k-\ell)!\ell!$. And $\ell+1$ and $k-\ell+1$ are odd integers; that is, ℓ and k are even integers.

If the function $f(\xi,\chi)$ is sufficiently smooth, then

$$E[f]=\sum_{m=1}^{M}\sum_{k=1}^{n-1}\sum_{\ell=0}^{k}C_{k\ell m}\,\Delta\xi_m^{\ell+1}\Delta\chi_m^{k-\ell+1}+Rn$$

where $C_{k\ell m}=\dfrac{1}{2^k(\ell+1)!\,(k-\ell+1)!}\left(\dfrac{\partial}{\partial\xi}\right)^{\ell}\left(\dfrac{\partial}{\partial\chi}\right)^{k-\ell}f(\xi_m,\chi_m)<\infty.$

According to the partition rule of the discrete cones, $\Delta\chi_m=(\pi/2)/(N/2-i+1)$ for the m'th cone in the i'th ξ-level, and $\Delta\xi_m=\gamma_i/N$ for the i'th ξ-level where γ_i is a constant associated with the ξ-level. Hence,

$$|E[f]| \leq \left| \sum_{k=1}^{n-1} \sum_{\ell=0}^{k} C_{k\ell} \{ (\frac{\gamma_{N/2}}{N})^{\ell+1} (\frac{\pi}{2})^{k-\ell+1} + 2(\frac{\gamma_{N/2-1}}{N})^{\ell+1} (\frac{\pi/2}{2})^{k-\ell+1} + \ldots \right.$$

$$+ (\frac{N}{2} - i + 1)(\frac{\gamma_i}{N})^{\ell+1} (\frac{\pi/2}{N/2 - i + 1})^{k-\ell+1} + \ldots$$

$$\left. + \frac{N}{2} (\frac{\gamma_1}{N})^{\ell+1} (\frac{\pi/2}{N/2})^{k-\ell+1} \} \right| + |Rn|$$

$$= \left| \sum_{k=1}^{n-1} \sum_{\ell=0}^{k} C_{k\ell} \{ \frac{d_{N/2}}{N^{\ell+1}} + \ldots + \frac{d_i}{N^{\ell+1} (\frac{N}{2} - i + 1)^{k-\ell}} + \ldots + \frac{d_1}{N^{k+1}} \} \right| + |Rn|$$

where $C_{k\ell} = \max_{1 \leq m \leq M} \{C_{k\ell m}\}$ and $d_i = (\pi\gamma_i/2)^{k+2}$. Leaving only the most dominant term, $k = 2$, $\ell = 0$ and 2,

$$|E[f]| \leq \left| C_{20} \{ \frac{d_{N/2}}{N} + \ldots + \frac{d_i}{N(N/2 - i + 1)^2} + \ldots + \frac{d_1}{N^3} \} + C_{22} \{ \frac{d_{N/2}}{N^3} + \ldots \right.$$

$$\left. + \frac{d_i}{N^3} + \ldots + \frac{d_1}{N^3} \} \right| \leq \frac{C}{N} .$$

This completes the proof.

Proof of Theorem 2.2. By the definitions,

$$|J - J_{DTR}| = \left| \iint (\underline{\Omega} \cdot \underline{n}) \, f(\underline{\Omega}) \, d\underline{\Omega} - \sum_{m=1}^{M} \left(\iint_{\Delta\Omega_m} \underline{\Omega} \cdot \underline{n} \, d\underline{\Omega} \right) f(\underline{\Omega}_m) \right|$$

$$\leq \left| \iint (\underline{\Omega} \cdot \underline{n}) \, f(\underline{\Omega}) \, d\underline{\Omega} - \sum_{m=1}^{M} \xi_m w_m f(\underline{\Omega}_m) \right| + \left| \sum_{m=1}^{M} \xi_m w_m f(\underline{\Omega}_m) - \right.$$

$$\left. - \sum_{m=1}^{M} \left(\iint_{\Delta\Omega_m} \underline{\Omega} \cdot \underline{n} \, d\underline{\Omega} \right) f(\underline{\Omega}_m) \right|$$

where we define the coordinate system of the direction vector $\underline{\Omega}$ so that

$\underline{\Omega}\cdot\underline{n} = \xi$. If we regard $\underline{\Omega}\cdot\underline{n}f(\underline{\Omega})$ as a function, the first term of the above inequality is smaller than C/N by Theorem 2.1.

By performing the integration, the second term of the inequality becomes

$$\left| \sum_{m=1}^{M} (\xi_m w_m f(\underline{\Omega}_m) - \int_{\xi_-}^{\xi_+}\int_{\chi_-}^{\chi_+} \xi \, d\xi d\chi \, f(\underline{\Omega}_m)) \right| = \left| \sum_{m=1}^{M} (\xi_m w_m - \frac{1}{2}(\xi_+^2 - \xi_-^2) \times (\chi_+ - \chi_-))f(\underline{\Omega}_m) \right| = \left| \sum_{m=1}^{M} (\xi_m w_m - \frac{\xi_+ + \xi_-}{2}(\xi_+ - \xi_-)(\chi_+ - \chi_-)f(\underline{\Omega}_m) \right| .$$

Since $w_m = \int_{\xi_-}^{\xi_+}\int_{\chi_-}^{\chi_+} d\xi d\chi = (\xi_+ - \xi_-)(\chi_+ - \chi_-)$ and $\xi_m = \frac{1}{2}(\xi_+ + \xi_-)$, this term vanishes. Therefore, the desired inequality is obtained.

It is noted that in order to prove the above theorems we made assumption that $\xi_m = \frac{1}{2}(\xi_{m+1/2} + \xi_{m-1/2})$ and $\chi_m = \frac{1}{2}(\chi_{m+1/2} + \chi_{m-1/2})$. This assumption, generally, is not correct; however, these relations are nearly correct as long as the EQ_N quadrature set is used. Meanwhile, the smoothness of the integrand holds for most of the problems except streaming problems where the angular flux may be a discontinuous function with respect to the direction variables rather than a continuous function. Some of these situations will be demonstrated in later chapters. Therefore, the above theorems tell us only very rough estimates for the numerical convergence of the double triangle rules, and more strict error estimates are desired.

Numerical examples of the integrations by the EQ_N quadrature and the double triangle rule are shown in Tables 2.4(a) and 2.4(b) for the scalar flux defined by Eq. (2.1) and the current defined by Eq. (2.10), respectively.

As for the scalar flux, the accuracy of the two methods is the same as we described. Table 2.4(a) (1) shows error for a fourth power polynomial

Table 2.4(a). Error Constants for the Numerical Integration of the Scalar Flux

(1) Exact Solution, 1.0471975512E-01 by d01fcf in NAG lib.

$f(\eta,\omega) = \mu^2\xi^2 = (1 - \eta^2)^2 \cos^2\omega \sin^2\omega$

N	EQ_N	ERROR*2)	DTR	ERROR
2	1.7453291E-01	6.9813151E-02	1.7453291E-01	6.9813151E-02
4	1.0471975E-01	2.8340055E-09	1.0471975E-01	1.7868085E-09
6	1.0471976E-01	4.8847149E-10	1.0471976E-01	4.6772617E-09
8	1.0471974E-01	1.5729555E-08	1.0471974E-01	1.5739555E-08
10	1.0471976E-01	8.3265972E-10	1.0471977E-01	1.1304636E-08
12	1.0471976E-01	4.8758348E-09	1.0471976E-01	6.2371917E-09
14	1.0471976E-01	1.2347590E-10	1.0471976E-01	2.2178708E-09
16	1.0471976E-01	4.5225939E-08	1.0471974E-01	1.5904412E-08

(2) Exact Soultion = 1.8155269706E+00 by d01fcf in NAG lib.

$f(\eta,\omega) = \eta^2 + \omega^2 \neq \sum_{k\ell} \mu^k \xi^\ell c_{k\ell}$

N	EQ_N	ERROR	DTR	ERROR
2	1.4925448E+00	3.2298219E-01	1.4925448E+00	3.2298219E-01
4	1.6621539E+00	1.5337304E-01	1.6621540E+00	1.5337302E-01
6	1.7218618E+00	9.3665169E-02	1.7218619E+00	9.3665100E-02
8	1.7517012E+00	6.3825775E-02	1.7218619E+00	6.3825775E-02
10	1.7690654E+00	4.6461555E-02	1.7690656E+00	4.6461378E-02
12	1.7800497E+00	3.5477258E-02	1.7800497E+00	3.5477235E-02
14	1.7874495E+00	2.8077471E-02	1.7874495E+00	2.8077435E-02
16	1.7927131E+00	2.2813872E-02	1.7927136E+00	2.2813370E-02

Table 2.4(b). Error Constants for the Numerical Integrations of the Current

(1) Ans = 7.8539816340E-01 by d01fcf in NAG lib.

$f(\eta,\omega) = 1$

N	EQ_N	ERROR	DTR	ERROR
2	9.0689973E-01	1.2150157E-01	7.8539816E-01	7.1054274E-15
4	8.2149123E-01	3.6093069E-02	7.8539816E-01	0.
6	8.0473042E-01	1.9332256E-02	7.8539816E-01	0.
8	7.9709725E-01	1.1699087E-02	7.8539816E-01	1.0658141E-14
10	7.9342884E-01	8.0307740E-03	7.8539816E-01	1.4210855E-14
12	7.9116440E-01	5.7652334E-03	7.8539816E-01	2.8421709E-14
14	7.8978883E-01	4.3903712E-03	7.8539816E-01	1.7763568E-14
16	7.8883480E-01	3.4256336E-03	7.8539816E-01	2.1316282E-14

(2) Ans = 1.9634954085E-01 by d01fcf in NAG lib.

$f(\eta,\omega) = \eta^2 \sin^2\omega$

N	EQ_N	ERROR	DTR	ERROR
2	1.5114995E-01	4.5199594E-02	1.3089969E-01	6.5449854E-02
4	1.9419019E-01	2.1593483E-03	1.8509183E-01	1.0257711E-02
6	1.9576015E-01	5.8938693E-04	1.9193771E-01	4.4118349E-03
8	1.9614589E-01	2.0365142E-04	1.9386985E-01	2.4796894E-03
10	1.9625467E-01	9.4869482E-05	1.9472657E-01	1.6229721E-03
12	1.9630177E-01	4.7772441E-05	1.9518996E-01	1.1595768E-03
14	1.9632193E-01	2.7606493E-05	1.9546717E-01	8.8236686E-04
16	1.9633284E-01	1.6703276E-05	1.9564805E-01	7.0149157E-04

(3) Ans = 5.8904862255E-01 by d01fcf in NAG lib.

$$f(\eta,\omega) = \begin{cases} 1 & 1/2 \leq \eta \leq 1 \\ 0 & 0 \leq \eta \leq 1/2 \end{cases}$$

N	EQ_N	ERROR	DTR	ERROR
2	9.0689973E-01	3.1785111E-01	7.8539816E-01	1.9634954E-01
4	4.5494989E-01	1.3409873E-01	4.3633231E-01	1.5271631E-01
6	6.0088554E-01	1.1836921E-02	5.8904862E-01	3.5527137E-15
8	6.6812353E-01	7.9074908E-02	6.5973446E-01	7.0685835E-02
10	5.0587601E-01	8.3172617E-02	5.0265482E-01	8.6393798E-02
12	5.7251442E-01	1.6534202E-02	5.6990343E-01	1.9145193E-02
14	6.1828103E-01	2.9232406E-02	6.1609677E-01	2.7048151E-02
16	6.0946771E-01	2.0419091E-02	6.0541108E-01	1.6362462E-02

*1) NAG Library, Numerical Algorithm Group (1981)

*2) ERROR = | solution - exact solution |

equation, $\mu^2\xi^2$. The approximations give essentially exact answers provided N is larger than four. The table demonstrates this. The discrepancy between errors of the EQ_N quadrature and the DTR is due to floating errors; in fact, the number of the significant digits of the quadrature data is only seven. On the other hand, if the integrand such as a function $\eta^2 + \omega^2$ is not in the form $\mu^k\xi^\ell$, the error becomes large. This example is shown in Table 2.4(a) (2), where the error is about 0.02 even for the 16th order of approximation.

As for the current, three examples are shown for integrals in the R-Z coordinate system. The first case, Table 2.4(b) (1), is for a constant function over the octant. The DTR is exact; but the EQ_N quadrature has larger errors. For the second case, Table 2.4(b) (2), a smooth function, $f = \eta^2 \sin^2\omega$ is used. The convergence rate defined as (error of the n'th order approximation)/(error of the (2n)'th order approximation) is about 20 for the EQ_N quadrature, and it is about 5 for the DTR. The latter rate is somewhat faster than that expected by Theorem 2.2, which predicts 2 as the convergence rate.

The two approximations are unsatisfactory for a discontinuous function as shown in Table 2.4(b) (3). For this example, a step function is defined by

$$f(\eta,\omega) = \begin{cases} 1 & 1/2 \leq \eta \leq 1 \\ 0 & 0 \leq \eta < 1/2 \end{cases} .$$

The errors are about 0.02 or larger except the error of the DC_6 approximation. The DC_6 approximation results in an exact integration, but it is rather accidental. In other words, we can choose the cone boundaries so that the DTR is exact for a step function. However, such a selection is not practical because the form of the step function is unknown until we solve the transport equation.

In conclusion, the double triangle rule results in satisfactory accuracy for the numerical integrations. If it fails, so does the EQ_N quadrature.

References for Section 2

1. B.G. Carlson, "Tables of Equal Weight Quadrature EQ_n over the Unit Sphere," Los Alamos Scientific Laboratory LA-4734 (1971).

2. G.I. Bell and S. Glasstone, "Nuclear Reactor Theory," Chapters 4 and 5, Robert E. Krieger Pub. Co., New York (1979).

3. J.J. Duderstadt and W.R. Martin, "Transport Theory," p. 516, Eq. (8.82), John Wiley & Sons, Inc., New York (1979).

4. R. Sanchez and N.J. McCormick, "A Review of Neutron Transport Approximations," Nucl. Sci. Eng. 80, 481-55 (1982).

5. K.D. Lathrop and F.W. Brinkley, "TWOTRAN-II: An Interface, Exportable Version of the TWOTRAN Code for Two-Dimensional Transport," Los Alamos Scientific Laboratory LA-4848-MS (1973).

3. THE DISCRETE CONES METHOD FOR VOIDS IN X-Y GEOMETRY

3.1 The Discrete Cones Method for a Mesh Cell (The DCS Method)

In this chapter, the discrete cones method will be applied to a solution of the transport equation in a void:

$$\Psi(\underline{r},\underline{\Omega}) = \int_0^{s_o} ds\, Q(\underline{r}-s\underline{\Omega},\underline{\Omega}) + \Psi(\underline{r}-s_o\underline{\Omega},\underline{\Omega}) \tag{3.1}$$

where s_o is the distance between two spatial points arranged on a characteristic line in the direction $\underline{\Omega}$.

To find the transfer matrix elements, we shall solve Eq. (3.1) for a rectangular mesh cell in an X-Y coordinate system as illustrated in Fig. 3.1. First, the solution is restricted to the direction satisfying $\xi > 0$ and $\pi/2 > \psi > 0$. Here, ξ is the direction cosine in the Z direction. Equation (3.1) is multiplied by $\underline{\Omega}\cdot\underline{n}_T$ and integrated over a cone m and the surface TOP. The result is

$$\begin{aligned}\int_{x_L}^{x_R} dx \iint_{\Delta\Omega_m} \underline{\Omega}\cdot\underline{n}_T\, \Psi(\underline{r}_T,\underline{\Omega})\, d\underline{\Omega} &= \int_{x_L}^{x_R} dx \iint_{\Delta\Omega_m} \underline{\Omega}\cdot\underline{n}_T\, d\underline{\Omega} \int_0^{s_o} ds\, Q(\underline{r}_T-s\underline{\Omega},\underline{\Omega}) \\ &+ \int_{x_L}^{x_R} dx \iint_{\Delta\Omega_m} \underline{\Omega}\cdot\underline{n}_T\, \Psi(\underline{r}-s_o\underline{\Omega},\underline{\Omega})\, d\underline{\Omega}\ ,\end{aligned} \tag{3.2}$$

where $\underline{r}_T$ is on the surface TOP, $\underline{n}_T$ is a unit vector normal to the surface TOP, $\Delta\Omega_m = [\xi_{m-1/2},\xi_{m+1/2}] \times [\psi_{m-1/2},\psi_{m+1/2}]$, and s_o is the distance between a point A on the surface TOP and the point where the characteristic line subtended from the point A intersects one of the boundary surfaces of the cell. To simplify the solution, we make the following assumptions:

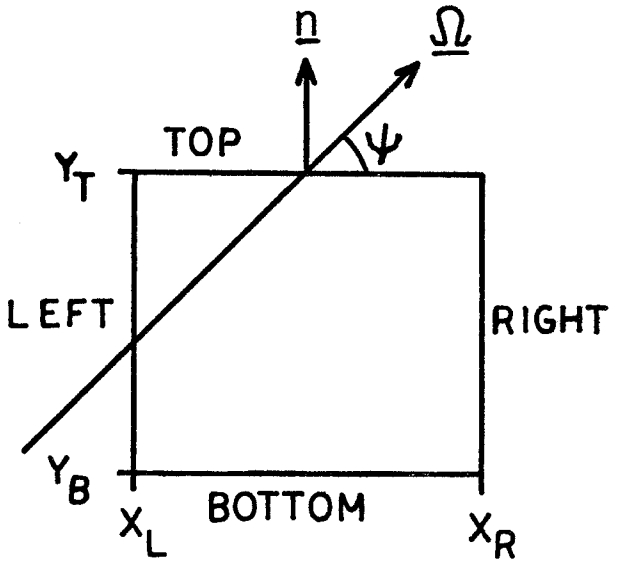

Fig. 3.1. Void geometry for the DCS method.

1. The angular flux $\Psi(\underline{r},\underline{\Omega})$ and the external source $Q(\underline{r},\underline{\Omega})$ are constant over a cone m;
2. $\Psi(\underline{r},\underline{\Omega})$ is constant on each of four boundary surfaces; and
3. $Q(\underline{r},\underline{\Omega})$ is constant in the spatial mesh cell.

These assumptions lead to

$$\Delta x\left(\iint_{\Delta\Omega_m} \underline{\Omega}\cdot\underline{n}_T \, d\underline{\Omega}\right)\Psi_{Tm} = \left(\int_{x_L}^{x_R} dx \iint_{\Delta\Omega_m} \underline{\Omega}\cdot\underline{n}_T s_o(x,\underline{\Omega}) \, d\underline{\Omega}\right)Q_m + \left(\int_{x_L}^{x_R} dx \iint_{\Delta\Omega_m} \underline{\Omega}\cdot\underline{n}_T\right)\Psi_m^- \tag{3.3}$$

where $\Delta x = x_R - x_L$, Ψ_{Tm} is the m'th cone flux on the surface TOP, and Ψ_m^- is the m'th cone flux on either the surface LEFT or BOTTOM.

In the remainder of this section, $\xi_{m\pm1/2}$ and $\psi_{m\pm1/2}$ will be abbreviated to $\xi_\pm$ and $\psi_\pm$, respectively. By the definition, $\underline{\Omega}\cdot\underline{n}_T = \sqrt{1-\xi^2}\sin\psi$. Hence, the left-hand side of Eq. (3.3) becomes

$$\text{L.H.S.} = \Delta x g_m(\cos\psi_- - \cos\psi_+)\Psi_{Tm} \tag{3.4}$$

where

$$g_m = \int_{\xi_-}^{\xi_+} \sqrt{1-\xi^2}\, d\xi \, .$$

To go further, we define ψ_o, ψ_1, x_1, and x_2 by $\psi_o = \arctan\left(\frac{\Delta y}{\Delta x}\right)$, $\tan\psi_1 = \frac{\Delta y}{x - x_L}$, $\tan\psi_+ = \frac{\Delta y}{x_1 - x_L}$, and $\tan\psi_- = \frac{\Delta y}{x_2 - x_L}$. Examining the geometry illustrated in Fig. 3.1 carefully, we find that

i) for $\psi_o > \psi_+$, all particles on TOP cross LEFT,

ii) for $\psi_+ > \psi_o > \psi_-$, particles with $x\varepsilon[x_L,x_1]$ on TOP cross LEFT; meanwhile, particles with $x\varepsilon[x_1,x_R]$ on TOP cross LEFT if the direction ψ satisfies $\psi_- < \psi < \psi_1$, and they cross BOTTOM if not,

iii) for $\psi_- > \psi_0$, particles with $x\varepsilon[x_L,x_1]$ on TOP cross LEFT, and particles with $x\varepsilon[x_2,x_R]$ on TOP cross BOTTOM; meanwhile, particles with $x\varepsilon[x_1,x_2]$ on TOP cross LEFT if the direction ψ satisfies $\psi_- < \psi < \psi_1$, and they cross BOTTOM if not.

In addition, we can obtain explicit formulas for s_0. If a particle in direction $\underline{\Omega} = (\xi,\psi)$ at x on TOP crosses LEFT, s_0 is given by $s_0 = (x - x_L)/(\sqrt{1 - \xi^2}\cos\psi)$. On the other hand, if it crosses BOTTOM, $s_0 = \Delta y/(\sqrt{1 - \xi^2}\sin\psi)$ where $\Delta y = y_T - y_B$. Taking all of the above relations into account, we have the following expressions for the right-hand side of Eq. (3.3):

For $\psi_0 > \psi_+$,

$$\text{R.H.S.} = \left(\int_{x_L}^{x_R} dx \int_{\psi_-}^{\psi_+} d\psi \sin\psi\right)\left(g'_m \frac{x - x_L}{\cos\psi} Q_m + g_m \Psi_{Lm}\right) . \qquad (3.5a)$$

For $\psi_+ > \psi_0 > \psi_-$,

$$\text{R.H.S.} = \left(\int_{x_L}^{x_R} dx \int_{\psi_-}^{\psi_+} d\psi \sin\psi + \int_{x_1}^{x_R} dx \int_{\psi_-}^{\psi_1} d\psi \sin\psi\right)\left(g'_m \frac{x - x_L}{\cos\psi} Q_m + g_m \Psi_{Lm}\right) \qquad (3.5b)$$
$$+ \left(\int_{x_L}^{x_R} dx \int_{\psi_1}^{\psi_+} d\psi \sin\psi\right)\left(g'_m \frac{\Delta y}{\sin\psi} Q_m + g_m \Psi_{Bm}\right) .$$

For $\psi_- > \psi_0$,

$$\text{R.H.S.} = \left(\int_{x_L}^{x_1} dx \int_{\psi_-}^{\psi_+} d\psi \sin\psi + \int_{x_1}^{x_2} dx \int_{\psi_-}^{\psi_1} d\psi \sin\psi\right)\left(g'_m \frac{x - x_L}{\cos\psi} Q_m + g_m \Psi_{Lm}\right)$$
$$+ \left(\int_{x_1}^{x_2} dx \int_{\psi_1}^{\psi_+} d\psi \sin\psi \right. \qquad (3.5c)$$
$$\left. + \int_{x_2}^{x_R} dx \int_{\psi_-}^{\psi_+} d\psi \sin\psi\right)\left(g'_m \frac{\Delta y}{\sin\psi} Q_m + g_m \Psi_{Bm}\right) .$$

Here $g'_m = \int_{\xi_-}^{\xi_+} d\xi = \xi_+ - \xi_-$, and Ψ_{Lm} and Ψ_{Bm} are the m'th cone fluxes on the surfaces LEFT and BOTTOM, respectively.

From Eq. (3.4) and Eqs. (3.5), three equations are obtained. Dividing both sides of these equations by $\Delta x g_m(\cos\psi_- - \cos\psi_+)$ results in a general equation

$$\Psi_{Tm} = T_{TBm}\Psi_{Bm} + T_{TLm}\Psi_{Lm} + P_{Tm}Q_m \qquad (3.6)$$

where T_{TBm}, T_{TLm}, and P_{Tm} are the elements of the transfer and escape matrices. Performing all the integrations in Eqs. (3.5) analytically leads to the following expressions for the transfer and escape matrix elements.

For $\psi_o \geq \psi_+$,

$$T_{TBm} = 1.0$$
$$P_{Tm} = \frac{g'_m}{g_m} \frac{\Delta x \ln(\cos\psi_-/\cos\psi_+)}{2(\cos\psi_- - \cos\psi_+)} . \qquad (3.7a)$$

For $\psi_+ > \psi_o \geq \psi_-$,

$$T_{TBm} = \frac{\frac{1}{\cos\psi_o} - \frac{\tan\psi_o}{\sin\psi_-} - \left(1 - \frac{\tan\psi_o}{\tan\psi_+}\right)\cos\psi_+}{\cos\psi_- - \cos\psi_+}$$

$$P_{Tm} = \frac{g'_m}{g_m} \frac{\Delta y^2\left\{\frac{\ln(\cos\psi_-)}{\tan^2\psi_o} - \frac{\ln(\cos\psi_o)}{\sin^2\psi_o} + \frac{2(\psi_+ - \psi_o)}{\tan\psi_o} + \ln\left(\cos\psi_o \frac{\sin\psi_o}{\sin\psi_+}\right)\right\}}{2\Delta x(\cos\psi_- - \cos\psi_+)} \quad (3.7b)$$

For $\psi_- > \psi_o$,

$$T_{TBm} = \frac{\left(1 - \frac{\tan\psi_o}{\tan\psi_-}\right)\cos\psi_- + \tan\psi_o\left(\frac{1}{\sin\psi_-} - \frac{1}{\sin\psi_+}\right) - \left(1 - \frac{\tan\psi_o}{\tan\psi_+}\right)\cos\psi_+}{\cos\psi_- - \cos\psi_+}$$

$$P_{Tm} = \frac{g'_m}{g_m} \frac{\Delta y^2\left\{\frac{2(\psi_+ - \psi_-)}{\tan\psi_o} + \ln\left(\frac{\sin\psi_-}{\sin\psi_+}\right)\right\}}{2\Delta X(\cos\psi_- - \cos\psi_+)} . \quad (3.7c)$$

For all the cases, $T_{TLm} = 1 - T_{TBm}$.

In the same manner, we can obtain the cone flux on the surface RIGHT. The equation corresponding to Eq. (3.6) is now,

$$\Psi_{Rm} = T_{RLm}\Psi_{Lm} + T_{RBm}\Psi_{Bm} + P_{Rm}Q_m . \quad (3.8)$$

Here, T_{RLm} and P_{Rm} are given by the following equations.

For $\psi_o > \psi_+$,

$$T_{RLm} = \frac{\left(1 - \frac{\tan\psi_+}{\tan\psi_o}\right)\sin\psi_+ + \frac{1}{\tan\psi_o}\left(\frac{1}{\cos\psi_+} - \frac{1}{\cos\psi_-}\right) - \left(1 - \frac{\tan\psi_-}{\tan\psi_o}\right)\sin\psi_-}{\sin\psi_+ - \sin\psi_-}$$

$$P_{Rm} = \frac{g_m'}{g_m} \frac{\left\{2(\psi_+ - \psi_-)\tan\psi_o + \ln\left(\frac{\cos\psi_+}{\cos\psi_-}\right)\right\}}{2\Delta X(\sin\psi_+ - \sin\psi_-)} . \qquad (3.9a)$$

For $\psi_+ > \psi_o > \psi_-$,

$$T_{RLm} = \frac{\frac{1}{\sin\psi_o} - \frac{1}{\tan\psi_o \cos\psi_-} - \left(1 - \frac{\tan\psi_-}{\tan\psi_o}\right)\sin\psi_-}{\sin\psi_+ - \sin\psi_-}$$

$$P_{Rm} = \frac{g_m'}{g_m} \frac{\Delta x^2\left\{2(\psi_o - \psi_-)\tan\psi_o + \tan^2\psi_o \ln(\sin\psi_+) - \frac{\ln(\sin\psi_o)}{\cos^2\psi_o} + \ln\left(\sin\psi_o \frac{\cos\psi_o}{\cos\psi_-}\right)\right\}}{2\Delta y(\sin\psi_+ - \sin\psi_-)} \qquad (3.9b)$$

For $\psi_- > \psi_o$,

$$T_{RLm} = 1.0$$

$$P_{Rm} = \frac{g_m'}{g_m} \frac{\Delta X^2\left\{2(\psi_+ - \psi_-)\tan\psi_o + \ln\left(\frac{\cos\psi_+}{\cos\psi_-}\right)\right\}}{2\Delta y(\sin\psi_+ - \sin\psi_-)} . \qquad (3.9c)$$

And, for all the cases, $T_{RBm} = 1 - T_{RLm}$.

In X-Y geometry, the direction space is symmetrical about the $\mu - \eta$ plane; hence, only a hemisphere of the unit sphere of directions must be considered. In other words, we consider the particles streaming in four quad-

rants, which are a projection of the hemisphere onto $\mu - \eta$ plane. These quadrants are numbered as shown in Fig. 3.2. Since we have already obtained the transfer and escape matrix elements of quadrant I, we must find the elements of the three other quadrants. To do so, first recall that we partition the four octants of the unit sphere of directions so that the cones are symmetrical about $\mu - \xi$ and $\eta - \xi$ planes. Using this symmetry, we find the following relations between the transfer matrix elements of different quadrants:

$$
\begin{aligned}
&T_{TRm'} = T_{TLm},\ T_{TBm'} = T_{TBm},\ T_{LRm'} = T_{RLm},\ T_{RBm'} = T_{LBm}, \\
&T_{BLn'} = T_{LTm},\ T_{BTn'} = T_{TBm},\ T_{RLn'} = T_{RLm},\ T_{RTn'} = T_{RBm}, \\
&T_{BRm''} = T_{BLn'},\ T_{BTm''} = T_{BTn'},\ T_{LRm''} = T_{RLn'},\ T_{LTm''} = T_{RTn'}, \\
&P_{Tm'} = P_{Tm},\ P_{Lm'} = P_{Rm},\ P_{Bn'} = P_{Tm},\ P_{Bm''} = P_{Bn'},\ P_{Lm''} = P_{Rn'} ,
\end{aligned}
\tag{3.10}
$$

where $T_{k\ell m}$ indicates the transfer matrix elements of a particle streaming from surface ℓ to surface k in the m'th cone in quadrant I. In Eqs. (3.10), cones m' and m, and cones m'' and n' are mirror images of each other about the $\eta - \xi$ plane. Also, cones n' and m are mirror images of each other about the $\mu - \xi$ plane.

Having Eqs. (3.10), we can calculate all the cell edge fluxes by Eqs. (3.6) and (3.8). Although we do not need to know the cell average flux in a void for a solution of Eq. (3.1), we are interested in the flux. To find this, we may use any expression because the cell average flux does not affect the convergence of a solution. On this point, a solution in a void is different from the solution in a non-void where the cell average flux influences the scattering source. In the present method, the cell average flux is obtained by averaging four cell edge fluxes of a cone:

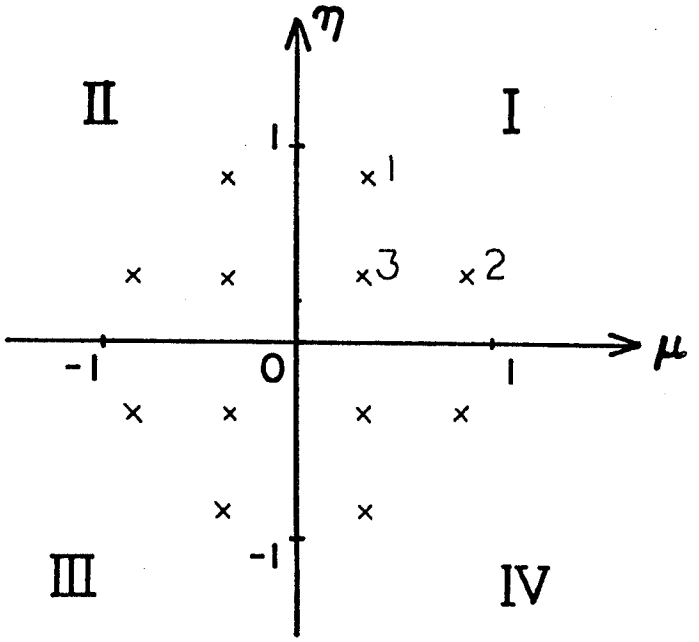

Fig. 3.2. The μ - η plane of directions and quadrature points for the DC_4 approximation.

$$\Psi_m = \frac{1}{4} (\Psi_{Tm} + \Psi_{Bm} + \Psi_{Lm} + \Psi_{Rm}) \ . \tag{3.11}$$

3.2 The Discrete Cones Method for a Void (The DCL Method)

In the preceding section, the transfer and escape matrix elements of a spatial mesh cell were obtained. In this section we shall find the transfer matrix elements of a void that is made up of many smaller mesh cells. The geometry of the void is illustrated in Fig. 3.3(a). To simplify the solution, we consider Eq. (3.1) without the source term:

$$\Psi(\underline{r},\underline{\Omega}) = \Psi(\underline{r}-s_o\underline{\Omega},\underline{\Omega}) \ . \tag{3.12}$$

Multiplying this by $\underline{\Omega}\cdot\underline{n}_T$ and integrating it over the m'th cone and the j'th subsurface on the surface TOP, we have

$$\int_{x_{j-1/2}}^{x_{j+1/2}} dx \iint_{\Delta\Omega_m} d\underline{\Omega}\ \underline{\Omega}\cdot\underline{n}_T\ \Psi(\underline{r}_T,\underline{\Omega}) = \int_{x_{j-1/2}}^{x_{j+1/2}} dx \iint_{\Delta\Omega_m} d\underline{\Omega}\ \underline{\Omega}\cdot\underline{n}_T\ \Psi(\underline{r}_T-s_o\underline{\Omega},\underline{\Omega}) \ . \tag{3.13}$$

If we assume that the angular flux is constant over the cone m and the subsurface j, then the left-hand side of Eq. (3.13) becomes

$$\Delta x_j g_m (\cos\psi_- - \cos\psi_+)\ \Psi_{Tjm} \tag{3.14}$$

where $\Delta x_j = x_{j+1/2} - x_{j-1/2}$ and $g_m = \int_{\xi_-}^{\xi_+} \sqrt{1-\xi^2}\, d\xi$. A characteristic line extended to an incoming surface from a point on the h'th subsurface of TOP crosses either the subsurface k on LEFT or the subsurface k' on BOTTOM. Furthermore, the characteristic line lies in the same cone on both the in-

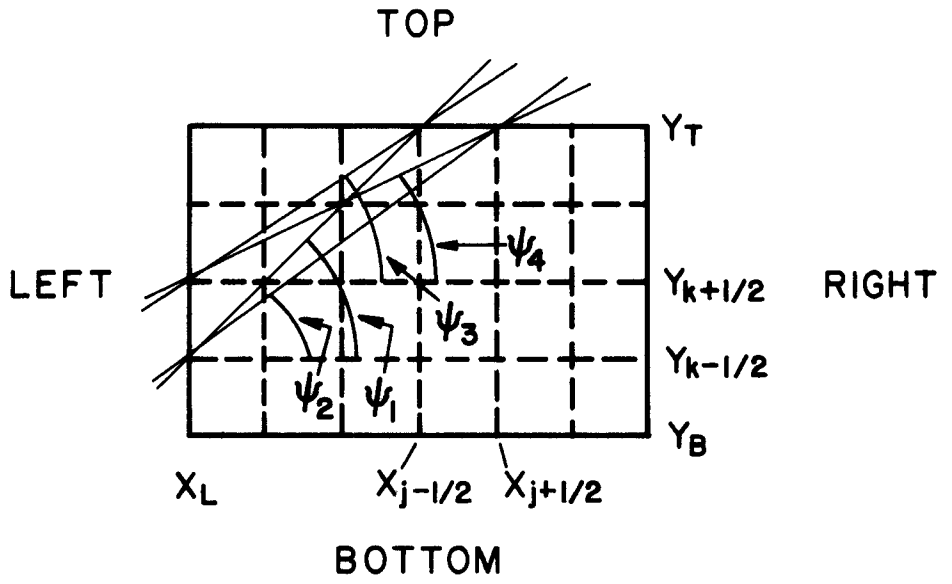

a)

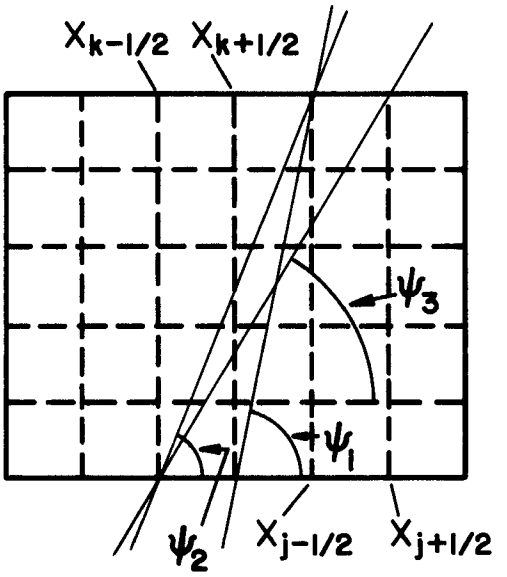

b)

Fig. 3.3 (a-b) Void geometry for the DCL method.

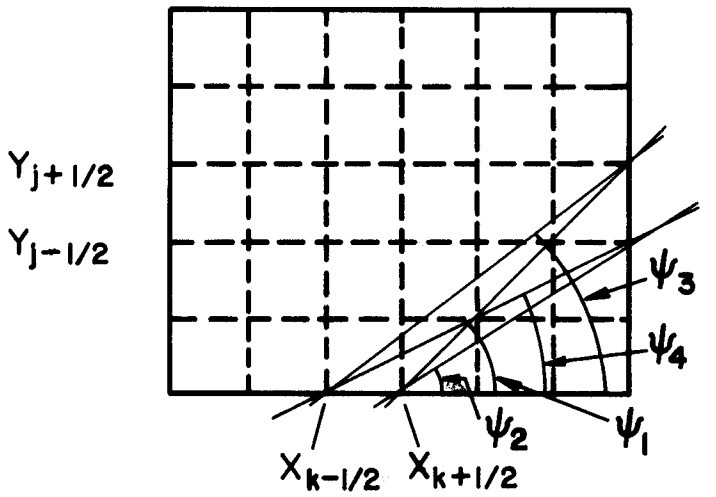

c)

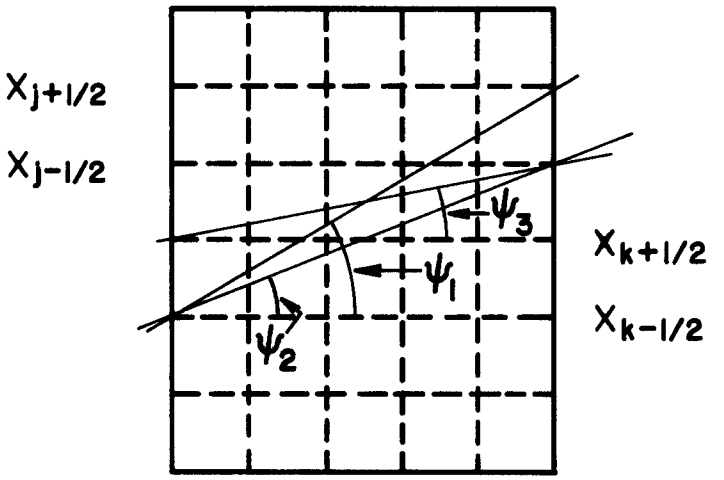

d)

Fig. 3.3 (c-d) Void geometry for the DCL method.

coming and outgoing surfaces. Taking account of these, we can represent the right-hand side of Eq. (3.13) as

$$\sum_k A_{mjk}\ \Psi_{Lkm} + \sum_{k'} B_{mjk'}\ \Psi_{Bk'm} \cdot$$

Here, the summations are taken over all possible subsurfaces. Equating this to Eq. (3.14) and dividing both sides by $\Delta x_j g_m(\cos \psi_- - \cos \psi_+)$, we have

$$\Psi_{Tjm} = \sum_k T_{TLjkm}\ \Psi_{Lkm} + \sum_{k'} T_{TBjk'm}\ \Psi_{Bk'm} \qquad (3.15)$$

where T_{TLjkm} and $T_{TBjk'}$ are the elements of the transfer matrices.

To obtain explicit formulas for the transfer matrix elements, first we define x_1, x_2, x_3, and x_4 by

$$\tan \psi_+ = \frac{y_T - y_{k+1/2}}{x_1 - x_L} ,$$

$$\tan \psi_+ = \frac{y_T - y_{k-1/2}}{x_2 - x_L} ,$$

$$\tan \psi_- = \frac{y_T - y_{k+1/2}}{x_3 - x_L} ,$$

and

$$\tan \psi_- = \frac{y_T - y_{k-1/2}}{x_4 - x_L} .$$

Also, ψ_1, ψ_2, ψ_3, and ψ_4 are defined as the angles shown in Fig. 3.3(a).

Since the integral with respect to ξ cancels, T_{TLjkm} and $T_{TBjk'm}$ can be represented in a form of

$$\frac{\int_{x_{j-1/2}}^{x_{j+1/2}} dx\,(\cos\psi_{min} - \cos\psi_{max})}{\Delta x_j(\cos\psi_- - \cos\psi_+)} \tag{3.16}$$

where ψ_{min} is the smallest ψ of overlap between the cone m and the cone subtended by the subsurface k on LEFT or the subsurface k' on BOTTOM at a point x on the subsurface j of TOP, and similarly ψ_{max} is the largest ψ. As can be easily observed in Fig. 3.3(a), $\psi_4 < \psi_3 < \psi_1$ and $\psi_4 < \psi_2 < \psi_1$; but either $\psi_3 < \psi_2$ or $\psi_3 > \psi_2$. Hence, these two cases must be considered separately. Careful examinations of Fig. 3.3(a) lead to expressions of ψ_{min} and ψ_{max}. These ψ_{min} and ψ_{max} are listed for the transfer matrix element T_{TLjkm} on Table 3.1(a) and (b). As seen on these tables, these depend on the order of six angles ψ_1, ψ_2, ψ_3, ψ_4, ψ_+, and ψ_-. Note that on the tables ψ_+ and ψ_- are abbreviated to + and −, respectively.

In the same manner, the transfer matrix elements of the right surface of the void are obtained in a form of

$$\frac{\int_{y_{j-1/2}}^{y_{j+1/2}} dy\,(\sin\psi_{max} - \sin\psi_{min})}{\Delta y_j(\sin\psi_+ - \sin\psi_-)} \tag{3.17}$$

where $\Delta y_j = y_{j+1/2} - y_{j-1/2}$, and the definition of ψ_{min} and ψ_{max} is the same as that of (3.16).

To see how to find ψ_{min} and ψ_{max}, we choose case 4 in Table 3.1(a): $\psi_- < \psi_4 < \psi_3 < \psi_2 < \psi_- < \psi_1$. For convenience, we call the points where a characteristic line in the direction $\underline{\Omega} = (\psi,\xi)$ crosses the top surface and the

Table 3.1(a). cos ψ_{min} and cos ψ_{max} of T_{TLjkm} for $\psi_4 < \psi_3 < \psi_2 < \psi_1$

Case	ψ_4	ψ_3	ψ_2	ψ_1		x	cos ψ_{min}	cos ψ_{max}
1	-+					$x_- < x < x_+$	0.0	0.0
2	-	+				$x_- < x < x_1$ $x_1 < x < x_+$	0.0 CS2	0.0 cos (+)
3	-		+			$x_- < x < x_+$	CS2	cos (+)
4	-			+		$x_- < x < x_2$ $x_2 < x < x_+$	CS2 CS2	cos (+) CS1
5	-				+	$x_- < x < x_+$	CS2	CS1
6		-+				$x_- < x < x_1$ $x_1 < x < x_3$ $x_3 < x < x_+$	0.0 CS2 cos (-)	0.0 cos (+) cos (+)
7		-	+			$x_- < x < x_3$ $x_3 < x < x_+$	CS2 cos (-)	cos (+) cos (+)
8		-		+		$x_- < x < x_3$ $x_3 < x < x_2$ $x_2 < x < x_+$	CS2 cos (-) cos (-)	cos (+) cos (+) CS1
9		-			+	$x_- < x < x_3$ $x_3 < x < x_+$	CS2 cos (-)	CS1 CS1
10			-+			$x_- < x < x_+$	cos (-)	cos (+)
11			-	+		$x_- < x < x_2$ $x_2 < x < x_+$	cos (-) cos (-)	cos (+) CS1
12			-		+	$x_- < x < x_+$	cos (-)	CS1
13				-+		$x_- < x < x_2$ $x_2 < x < x_4$ $x_4 < x < x_+$	cos (-) cos (-) 0.0	cos (+) CS1 0.0
14				-	+	$x_- < x < x_4$ $x_4 < x < x_+$	cos (-) 0.0	CS1 0.0
15					-+	$x_- < x < x_+$	0.0	0.0

Table 3.1(b). cos ψ_{min} and cos ψ_{max} of T_{TLjkm} for $\psi_4 < \psi_2 < \psi_3 < \psi_1$

Case	ψ_4	ψ_2	ψ_3	ψ_1		x	cos ψ_-	cos ψ_+
1	-+					$x_- < x < x_+$	0.0	0.0
2	-	+				$x_- < x < x_1$	0.0	0.0
						$x_1 < x < x_+$	CS2	cos (+)
3	-		+			$x_- < x < x_1$	0.0	0.0
						$x_1 < x < x_2$	CS2	cos (+)
						$x_2 < x < x_+$	CS2	CS1
4	-			+		$x_- < x < x_2$	CS2	cos (+)
						$x_2 < x < x_+$	CS2	CS1
5	-				+	$x_- < x < x_+$	CS2	CS1
6		-+				$x_- < x < x_1$	0.0	0.0
						$x_1 < x < x_3$	CS2	cos (+)
						$x_3 < x < x_+$	cos (-)	cos (+)
7		-	+			$x_- < x < x_1$	0.0	0.0
						$x_1 < x < x_3$	CS2	cos (+)
						$x_3 < x < x_2$	cos (-)	cos (+)
						$x_2 < x < x_+$	cos (-)	CS1
8		-		+		$x_- < x < x_2$	CS2	cos (+)
						$x_2 < x < x_3$	CS2	CS1
						$x_3 < x < x_+$	cos (-)	CS1
9		-			+	$x_- < x < x_3$	CS2	CS1
						$x_3 < x < x_+$	cos (-)	CS1
10			-+			$x_- < x < x_1$	0.0	0.0
						$x_1 < x < x_3$	CS2	cos (+)
						$x_3 < x < x_2$	cos (-)	cos (+)
						$x_2 < x < x_4$	cos (-)	CS1
						$x_4 < x < x_+$	0.0	0.0

Table 3.1(b). (Continued)

Case	ψ_4	ψ_2	ψ_3	ψ_1		x	cos ψ_-	cos ψ_+
11			-	+		$x_- < x < x_2$ $x_2 < x < x_3$ $x_3 < x < x_4$ $x_4 < x < x_+$	CS2 CS2 cos (-) 0.0	cos (+) CS1 CS1 0.0
12			-		+	$x_- < x < x_3$ $x_3 < x < x_4$ $x_4 < x < x_+$	CS2 cos (-) 0.0	CS1 CS1 0.0
13				-+		$x_- < x < x_2$ $x_2 < x < x_4$ $x_4 < x < x_+$	cos (-) cos (-) 0.0	cos (+) CS1 0.0
14				-	+	$x_- < x < x_4$ $x_4 < x < x_+$	cos (-) 0.0	CS1 0.0
15					-+	$x_- < x < x_+$	0.0	0.0

(1) $$CS1 = \frac{x - x_L}{\sqrt{(x - x_L)^2 + (y_T - y_{k-1/2})^2}}$$

$$CS2 = \frac{x - x_L}{\sqrt{(x - x_L)^2 + (y_T - y_{k+1/2})}}$$

(2) $x_\pm = x_{j\pm1/2}$

(3) $\cos(\pm) = \cos \psi_{m\pm1/2}$

(4) $\pm = \psi_{m\pm1/2}$

left surface $A(\psi)$ and $B(\psi)$, respectively. Since ψ_- is smaller than any ψ_i (i = 1, 2, 3 and 4), ψ must be larger than an angle ψ^*, which is larger than ψ_- and satisfies an equation:

$$\cos \psi^* = \frac{x - x_L}{\sqrt{(x - x_L)^2 + (y_T - y_{k+1/2})^2}}$$

(= CS2 in the tables). Hence $\psi_{min} = \psi^*$. On the other hand, since $\psi_2 < \psi_+ < \psi_1$, $B(\psi_+)$ is on the k'th subsurface if the x coordinate of $A(\psi)$ is smaller than x_2, which is defined by $\tan \psi_+ = (y_T - y_{k-1/2})/(x_2 - x_L)$. In other words, $\psi_{max} = \psi_+$. If x is larger than x_2, $B(\psi_+)$ is on the k-1'th subsurface. Therefore, ψ must be smaller than ψ_+ so that $B(\psi)$ is on the k'th subsurface. The largest ψ is in fact given by

$$\cos \psi_{max} = \frac{x - x_L}{\sqrt{(x - x_L)^2 + (y_T - y_{k-1/2})^2}}$$

(= CS1 in the tables).

Integrations of Eqs. (3.16) and (3.17) are performed analytically by using the explicit expressions of ψ_{min} and ψ_{max}. The results are tabulated on Tables 3.2 through 3.5, where the formulas of the numerators in Eq. (3.16) and (3.17) are listed.

The transfer matrix elements obtained above are for particles streaming in the first quadrant of the μ - η plane of directions. The elements of the other quadrants are obtained by taking account of symmetry similar to one described in Section 3.1. Now, suppose the boundary surface of a void is partitioned as illustrated in Fig. 3.3(a). For the first quadrant $\mu > 0$ and $\eta > 0$, and the intervals of the boundary surfaces are numbered by setting the origin

Table 3.2(a). T_{TL} for $\psi_3 < \psi_2$

ψ_1, ψ_2, ψ_3, and ψ_4 are defined in Fig. 3.3(a)

Case	ψ_4	ψ_3	ψ_2	ψ_1	NUMERATOR
1	-+				0.0
2	-	+			$F_+(x_+,x_1) - (x_+ - x_1)\cos(+)$
3	-		+		$F_+(x_+,x_-) - \Delta x_j\cos(+)$
4	-			+	$F_+(x_+,x_-) - F_-(x_+,x_2) - (x_2 - x_-)\cos(+)$
5	-				+ $F_+(x_+,x_-) - F_-(x_+,x_-)$
6		-+			$(x_+ - x_3)\cos(-) + F_+(x_3,x_1) - (x_+ - x_1)\cos(+)$
7		-	+		$(x_+ - x_3)\cos(-) + F_+(x_3,x_-) - \Delta x_j\cos(+)$
8		-		+	$(x_+ - x_3)\cos(-) + F_+(x_3,x_-) - F_-(x_+,x_2)$
9		-			+ $(x_+ - x_3)\cos(-) + F_+(x_3,x_-) - F_-(x_+,x_-)$
10			-+		$\Delta x_j(\cos(-) - \cos(+))$
11			-	+	$\Delta x_j\cos(-) - F_-(x_+,x_2) - (x_2 - x_-)\cos(+)$
12			-		+ $\Delta x_j\cos(-) - F_-(x_+,x_-)$
13				-+	$(x_4 - x_-)\cos(-) - F_-(x_4,x_2) - (x_2 - x_-)\cos(+)$
14				-	+ $(x_4 - x_-)\cos(-) - F_-(x_4,x_-)$
15					-+ 0.0

$$F_\pm(p,q) \equiv \sqrt{(p - x_L)^2 + (y_T - y_{k\pm1/2})^2} - \sqrt{(q - x_L)^2 + (y_T - y_{k\pm1/2})^2}$$

$$\cos(\pm) \equiv \cos\psi_{m\pm1/2}\ ,\ x_\pm \equiv x_{j\pm1/2}$$

Table 3.2(b). T_{TL} for $\psi_2 < \psi_3$

ψ_1, ψ_2, ψ_3, and ψ_4 are defined in Fig. 3.3(a)

Case	ψ_4	ψ_2	ψ_3	ψ_1		NUMERATORS
1	-+					0.0
2	-	+				$F_+(x_+,x_1) - (x_+ - x_1)\cos(+)$
3	-		+			$F_+(x_+,x_-) - F_-(x_+,x_2) - (x_2 - x_1)\cos(+)$
4	-			+		$F_+(x_+,x_-) - F_-(x_+,x_2) - (x_2 - x_-)\cos(+)$
5	-				+	$F_+(x_+,x_-) - F_-(x_+,x_-)$
6		-+				$(x_+ - x_3)\cos(-) + F_+(x_3,x_1) - (x_+ - x_1)\cos(+)$
7		-	+			$(x_+ - x_3)\cos(-) + F_+(x_3,x_1) - F_-(x_+,x_2) - (x_2 - x_1)\cos(+)$
8		-		+		$(x_+ - x_3)\cos(-) + F_+(x_3,x_-) - F_-(x_+,x_2) - (x_2 - x_-)\cos(+)$
9		-			+	$(x_+ - x_3)\cos(-) + F_+(x_3,x_-) - F_-(x_+,x_-)$
10			-+			$(x_4 - x_3)\cos(-) + F_+(x_3,x_1) - F_-(x_4,x_2) - (x_2 - x_1)\cos(+)$
11			-	+		$(x_4 - x_3)\cos(-) + F_+(x_3,x_-) - F_-(x_4,x_2) - (x_2 - x_-)\cos(+)$
12			-		+	$(x_4 - x_3)\cos(-) + F_+(x_3,x_-) - F_-(x_4,x_-)$
13				-+		$(x_4 - x_-)\cos(-) - F_-(x_4,x_2) - (x_2 - x_-)\cos(+)$
14				-	+	$(x_4 - x_-)\cos(-) - F_-(x_4,x_-)$
15					-+	0.0

Table 3.3. T_{TB}

ψ_1, ψ_2, and ψ_3 are defined in Fig. 3.3(b)

Case	ψ_3	ψ_2	ψ_1		NUMERATOR
1	-+				0.0
2	-	+			$F_-(x_+,x_1) - (x_+ - x_1)\cos(+)$
3	-		+		$F_-(x_+,x_-) - F_+(x_+,x_2) - (x_2 - x_-)\cos(+)$
4	-			+	$F_-(x_+,x_-) - F_+(x_+,x_-)$
5		-+			$F_-(x_3,x_1) + (x_+ - x_3)\cos(-) - (x_+ - x_1)\cos(+)$
6		-	+		$F_-(x_3,x_-) + F_+(x_+,x_2) + (x_+ - x_3)\cos(-) - (x_2-x_1)\cos(+)$
7		-		+	$(x_+ - x_3)\cos(-) + F_-(x_3,x_-) - F_+(x_+,x_-)$
8			-+		$(x_4 - x_-)\cos(-) - F_+(x_4,x_2) - (x_2 - x_-)\cos(+)$
9			-	+	$(x_4 - x_-)\cos(-) - F_+(x_4,x_-)$
10				-+	0.0

$$F_\pm(p,q) = \sqrt{(p - x_{k\pm1/2})^2 + \Delta y^2} - \sqrt{(q - x_{k\pm1/2})^2 + \Delta y^2}$$

$$x_\pm = x_{j\pm1/2}$$

$$\cos(\pm) = \cos \psi_{m\pm1/2}$$

$$\tan \psi_{m+1/2} = \frac{\Delta y}{x_1 - x_{k-1/2}}, \qquad \tan \psi_{m+1/2} = \frac{\Delta y}{x_2 - x_{k+1/2}}$$

$$\tan \psi_{m-1/2} = \frac{\Delta y}{x_3 - x_{k-1/2}}, \qquad \tan \psi_{m-1/2} = \frac{\Delta y}{x_4 - x_{k+1/2}}$$

Table 3.4(a). T_{RB} for $\psi_2 < \psi_3$

ψ_1, ψ_2, ψ_3, and ψ_4 are defined in Fig. 3.3(c)

Case	ψ_4	ψ_2	ψ_3	ψ_1		NUMERATORS
1	-+					0.0
2	-	+				$G_-(y_-,y_1) + (y_1 - y_-)\sin(+)$
3	-		+			$G_+(y_2,y_-)\sin(+) + G_-(y_1,y_-) - (y_1 - y_2)\sin(+)$
4	-			+		$(y_+ - y_2)\sin(+) + G_+(y_2,y_-) - G_-(y_+,y_-)$
5	-				+	$G_+(y_+,y_-) - G_-(y_+,y_-)$
6		-+				$(y_1 - y_-)\sin(+) - G_-(y_1,y_3) - (y_3 - y_-)\sin(-)$
7		-	+			$(y_1 - y_2)\sin(+) + G_+(y_2,y_-) - G_-(y_1,y_3)$ $- (y_3 - y_-)\sin(-)$
8		-		+		$(y_+ - y_2)\sin(+) + G_+(y_2,y_-) - G_-(y_+,y_3)$ $- (y_3 - y_-)\sin(-)$
9		-			+	$G_+(y_+,y_-) - G_-(y_+,y_3) - (y_3 - y_-)\sin(-)$
10			-+			$(y_1 - y_2)\sin(+) + G_+(y_2,y_4) - G_-(y_1,y_3)$ $- (y_3 - y_4)\sin(-)$
11			-	+		$(y_+ - y_2)\sin(+) + G_+(y_2,y_4) - G_-(y_+,y_3)$ $- (y_3 - y_4)\sin(-)$
12			-		+	$G_+(y_+,y_4) - G_-(y_+,y_3) - (y_3 - y_4)\sin(-)$
13				-+		$(y_+ - y_2)\sin(+) + G_+(y_2,y_4) - (y_+ - y_4)\sin(-)$
14				-	+	$G_+(y_+,y_4) - (y_+ - y_4)\sin(-)$
15					-+	0.0

$$G_{\pm}(p,q) = \sqrt{(x_R - x_{k\pm1/2})^2 + (p - y_B)^2} - \sqrt{(x_R - x_{k\pm1/2})^2 + (q - y_B)^2}$$

$$\sin(\pm) = \sin \psi_{m\pm1/2}\ , \qquad y_{\pm} = y_{j\pm1/2}$$

Table 3.4(b). T_{RB} for $\psi_3 < \psi_2$

ψ_1, ψ_2, ψ_3, and ψ_4 are defined in Fig. 3.3(c)

Case	ψ_4	ψ_3	ψ_2	ψ_1		NUMERATORS
1	-+					0.0
2	-	+				$(y_1 - y_-)\sin(+) - G_-(y_1,y_-)$
3	-		+			$\Delta y_j \sin(+) - G_-(y_+,y_-)$
4	-			+		$(y_+ - y_2)\sin(+) + G_+(y_2,y_-) - G_-(y_+,y_-)$
5	-				+	$G_+(y_+,y_-) - G_-(y_+,y_-)$
6		-+				$(y_1 - y_-)\sin(+) - G_-(y_1,y_3) - (y_3 - y_-)\sin(-)$
7		-	+			$\Delta y_j \sin(+) - G_-(y_+,y_3) - (y_3 - y_-)\sin(-)$
8		-		+		$(y_+ - y_2)\sin(+) + G_+(y_2,y_-) - G_-(y_+,y_3) - (y_3 - y_-)\sin(-)$
9		-			+	$G_+(y_+,y_-) - G_-(y_+,y_3) - (y_3 - y_-)\sin(-)$
10			-+			$\Delta y_j(\sin(+) - \sin(-))$
11			-	+		$(y_+ - y_2)\sin(+) + G_+(y_2,y_-) - \Delta y_j \sin(-)$
12			-		+	$G_+(y_+,y_-) - \Delta y_j \sin(-)$
13				-+		$(y_+ - y_2)\sin(+) + G_+(y_2,y_4) - (y_+ - y_4)\sin(-)$
14				-	+	$G_+(y_+,y_4) - (y_+ - y_4)\sin(-)$
15					-+	0.0

$$\tan \psi_{m+1/2} = \frac{y_1 - y_B}{x_R - x_{k-1/2}} \qquad \tan \psi_{m+1/2} = \frac{y_2 - y_B}{x_R - x_{k+1/2}}$$

$$\tan \psi_{m-1/2} = \frac{y_3 - y_B}{x_R - x_{k-1/2}} \qquad \tan \psi_{m-1/2} = \frac{y_4 - y_B}{x_R - x_{k+1/2}}$$

Table 3.5. T_{RL}

ψ_1, ψ_2, and ψ_3 are defined in Fig. 3.3(d)

Case	ψ_3	ψ_2	ψ_1		NUMERATORS
1	-+				0.0
2	-	+			$(y_1 - y_-)\sin(+) - G_+(y_1,y_-)$
3	-		+		$(y_+ - y_2)\sin(+) + G_-(y_2,y_-) - G_+(y_+,y_-)$
4	-			+	$G_-(y_+,y_-) - G_+(y_+,y_-)$
5		-+			$(y_1 - y_-)\sin(+) - G_+(y_1,y_3) - (y_3 - y_-)\sin(-)$
6		-	+		$(y_+ - y_2)\sin(+) + G_-(y_2,y_-) - G_+(y_+,y_3) - (y_3 - y_-)\sin(+)$
7		-		+	$G_-(y_+,y_-) - G_+(y_+,y_3) - (y_3 - y_-)\sin(-)$
8			-+		$(y_+ - y_2)\sin(+) + G_-(y_2,y_4) - (y_+ - y_4)\sin(-)$
9			-	+	$G_-(y_+,y_4) - (y_+ - y_4)\sin(-)$
10				-+	0.0

$$\tan \psi_{m+1/2} = \frac{y_1 - y_{k+1/2}}{\Delta x}$$

$$\tan \psi_{m+1/2} = \frac{y_2 - y_{k-1/2}}{\Delta x}$$

$$\tan \psi_{m-1/2} = \frac{y_3 - y_{k+1/2}}{\Delta x}$$

$$\tan \psi_{m-1/2} = \frac{y_4 - y_{k-1/2}}{\Delta x}$$

$$G_{\pm}(p,q) = \sqrt{\Delta x^2 + (p - y_{k\pm1/2})^2} + \sqrt{\Delta x^2 + (q - y_{k\pm1/2})^2}$$

of the system to the point (x_L,y_B). By regarding the point (x_R,y_B) as the origin and numbering the intervals in an increasing order in the direction of (x_L,y_B), we may use the same transfer matrix elements for the second quadrant: $\mu < 0$ and $\eta > 0$ as those of the first quadrant. For the third quadrant, the point (x_L,y_R) must be regarded as the origin, and the number of the interval of the boundary surface parallel to the Y axis increases as Y decreases. For the fourth quadrant, the origin is set to the point (x_R,y_T). In this way, we can find all the necessary transfer matrix elements from those of the first quadrant. Consequently, Tables 3.2 through 3.5 give sufficient data of the transfer matrix elements for actual numerical calculations by the present method.

In this method, the calculation of the cell average flux of a mesh cell in a void is not as straightforward as in the previous method. Also, the cell-edge flux produced by a source inside the void is not easily calculated.

3.3 Programs DCS, DCL, and TWODCXY

The preceding two methods were inserted in a two-dimensional discrete ordinates program STRMEX, which was written by T. Seed, now with the INESCO Company. The program is a concise version of a more standard S_N code, TWOTRAN,[1] which was developed at Los Alamos National Laboratory. Although the discrete cones method was finally inserted in the TWOTRAN program, most of the preliminary tests of the methods were performed by modified versions of STRMEX.

A program that applies the discrete cones method to a mesh cell in a void described in Section 3.1 is called DCS; meanwhile, a program that applies the discrete cones method to a void as described in Section 3.2 is called DCL.

A modified TWOTRAN, which applies the former method, is called TWODCXY. To modify the TWOTRAN program, the subprogram SNCON that provides symmetric quadrature sets is replaced by the subprogram EQNCON that provides the EQ_N quadrature set. The subprogram QUADSET that computes the cone boundaries and the subprogram ADJUST that computes the adjustment factors are called by the subprogram INPUT14. The subprogram GRND21 calls the subprogram VOID that calculates the transfer and escape matrix elements and stores them in a common array A. These transfer and escape matrix elements are used in the subprograms IN and OUT when the transport equation is solved in a void. The structure of the TWODCXY program is shown in Table 3.6.

The algorithm used by the programs will be explained in the remainder of this section. The programs calculate the transfer matrix elements before they start outer and inner iterations. The programs do the same outer iteration procedures over the energy groups and the eigenvalue search as those of the S_N code.[1] The inner iteration procedure sweeping spatial mesh cells and discrete directions is modified so that the discrete cones method is applied in a void.

For the DCS program as well as the TWODXCY program, the discrete ordinates flux (the DSN flux) is calculated cell by cell until a void is encountered. At the interface between a non-void cell and a void cell, incoming cone-fluxes (the DCN fluxes) are computed from the DSN fluxes by using the adjustment factors described in Chapter 2. Then, outgoing DCN fluxes of the void cell are obtained by using the incoming DCN fluxes and the transfer matrix elements. If the next cell is again a void, the outgoing DCN fluxes are regarded as the incoming DCN fluxes of the next cell. If the next cell is a non-void cell, the DSN fluxes are calculated from the outgoing DCN fluxes by

Table 3.6. Structure of the TWODCXY Program

OVERLAY (0,0)	OVERLAY (1,0)	OVERLAY (2,0)	OVERLAY (3,0)
TWODCXY[2]	INPUT1	GRIND2	OUTPUT3
1. MONITER	1. LOAD	1. REBAL	1. OUTPT31
2. ERROR	2. INPUT11[2]	2. GRIND21[2]	a. FINAL
3. CLEAR	a. DUMPRD	a. INITAL	2. OUTPUT32
4. MPLY	3. INPUT12	b. INITQ	a. EDCALL
5. WRITE	a. CSPREP	c. FISCAL	b. GENFLO
6. ECHECK	b. IFINXS	d. VOID[1]	c. EDITOR
7. DUMPER	4. INPUT13	3. GRIND22	d. EDMAP
8. PCMBAL	a. READQF	a. OUTER	3. IFOUT
9. REED	b. IFINQF	b. INNER[2]	a. IFRITE
10. RITE	5. INPUT14[2]	c. IN[2]	
	a. EQNCON[1]	d. OUT[2]	
	b. IFINSN	e. FIXUP	
	c. PNGEN	f. SETBC	
	d. QUADSET[1]	g. STORAF	
	e. ADJUST[1]	h. SAVEAF	
	6. INPUT15[2]	i. GSUMS	
	a. CSMESH	4. GRIND23	
	b. MAPPER	a. TESTS	
		b. NEWPAR	

1) These subprograms are newly added to the TWOTRAN-II program.

2) These subprograms are modified.

using the adjustment factors. The procedure is repeated over the inner iterations. The DCS program requires storage of 6×MM×IVOID transfer and escape matrix elements. Here MM is N(N + 2)/8 for the S_N approximation, and IVOID is the number of void cells that have a different spatial mesh size.

For the DCL program, the inner iteration is more complicated. After the DSN fluxes are computed cell by cell in non-voids, the DCN fluxes are computed by using the adjustment factors at the interface between a void and a non-void. Then, jumping up to the next void-non-void interface, all outgoing DCN fluxes of the subsurface are obtained from the incoming DCN fluxes by using the transfer matrix elements. The incoming DSN fluxes of the next non-void cell are computed from the outgoing DCN fluxes by using the adjustment factors. Since an outgoing DCN flux is related to the incoming DCN fluxes of many subsurfaces, the DCN fluxes of different subsurfaces must be stored for later use in the inner iteration. This increases the amount of memory required for an inner iteration. Furthermore, 4×MM×MS×NS transfer matrix elements must be stored for a solution of a void, which is divided into MS times NS subdomains.

The number of the transfer matrix elements increases considerably, compared with the DCS program; hence, a longer computing time for calculation of the elements results.

3.4 Numerical Results

PROBLEM 1

To demonstrate the computational characteristics of the discrete cones method, we present solutions for four problems.

The first problem is devised to demonstrate the ray streaming effect mitigation for the scalar flux distribution. The problem geometry is illus-

trated in Fig. 3.4. An isotropic uniform square neutron source is placed at the center of a domain. A vacuum region surrounds the source, around which a scattering material is placed. The outer boundaries are vacuum boundaries. The material has the macroscopic total cross section $\sigma_t = 0.2$, the macroscopic isotropic scattering cross section $\sigma_s = 0.19$, and the macroscopic absorption cross section $\sigma_a = 0.01$. The source region consists of the same material as the outer region. For convenience, a quarter of the problem is considered.

For the DCS, DCL, and DSN solutions, the region is divided into an 8 by 8 fine mesh. For the DCL solution, the inner vacuum region is divided into seven domains. The scalar flux distributions along the $x = 5.625$ cm plane by the DCS, DCL (both DC_8 approximations) and S_8 calculations are plotted in Fig. 3.4. A Monte Carlo solution by the MORSE code[2] is also plotted for reference.

The DCS and DCL solutions with the DC_8 approximation show the ray effect mitigations. The two solutions by DCS and DCL are almost identical. For another mesh specification, a 16 by 16 fine mesh, the CPU (Central Processor Unit) times for S_8, DCS and DCL (both DC_8 approximation) are 4.4, 4.2, and 12.4 seconds, respectively. The DCL method is inefficient in terms of CPU time.

PROBLEM 2

The second problem is a duct streaming problem. The geometry and material cross sections are shown in Fig. 3.5. The neutron source is isotropic. One-group calculations are carried out. The domain is divided into a 20 by 12 mesh. The vacuum region is divided into 4 subdomains for the DCL solution. The solutions by DSN, DCS and DCL are obtained varying the order of angle discretization. These solutions are compared with a solution by the MORSE code.

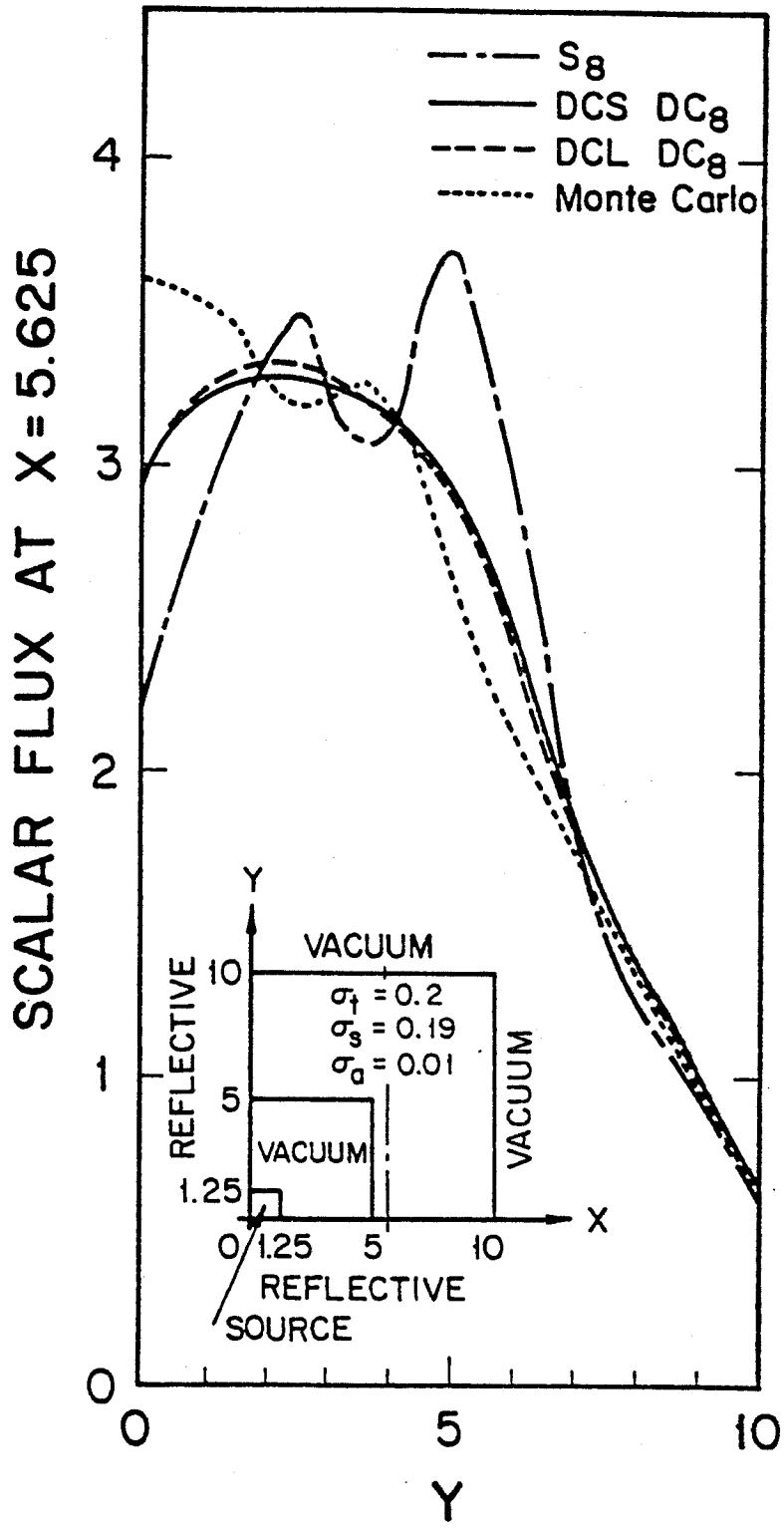

Fig. 3.4. Scalar flux distribution at x = 5.625 for Problem 1.

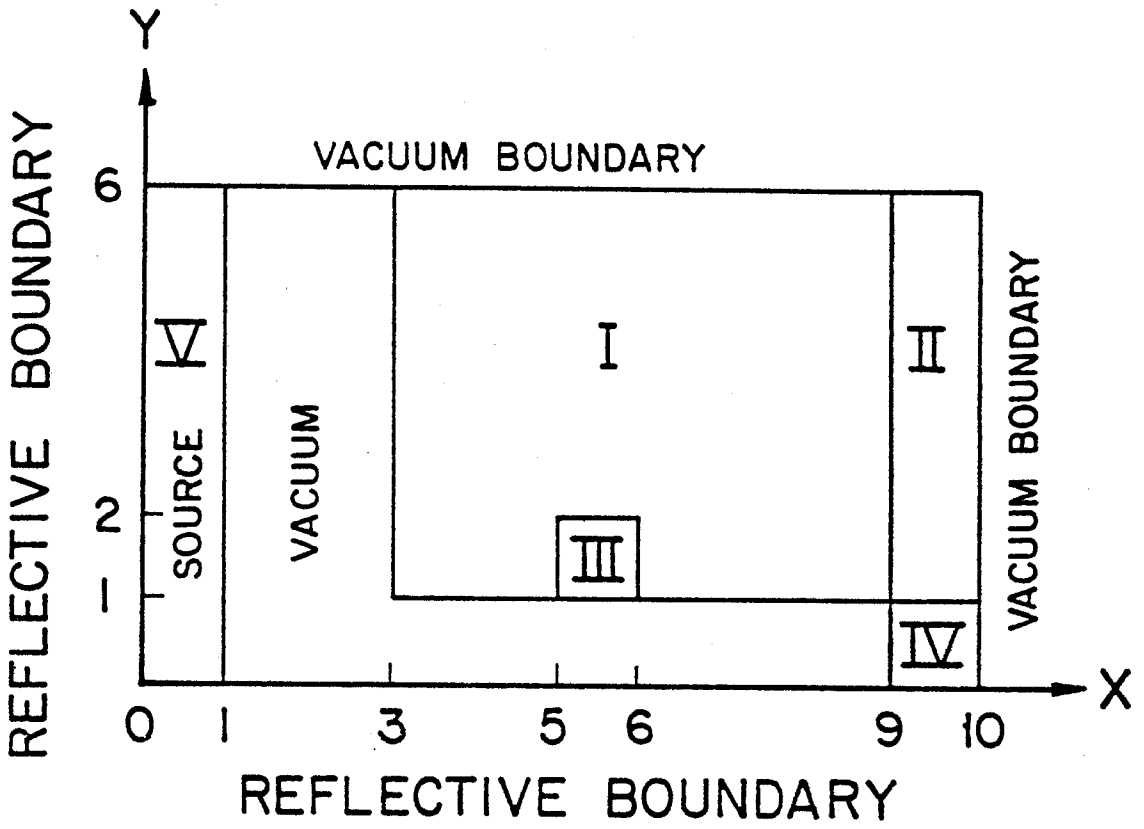

CROSS SECTIONS

MAT. No.	σ_a	$\nu\sigma_f$	σ_t	σ_s
I	0.1	0.0	1.0	0.9
II	0.5	0.0	2.0	1.5
III	0.1	0.0	1.0	0.9
IV	0.8	0.0	2.0	1.2
V	0.0	0.0	0.1	0.1

Fig. 3.5. Geometry and material cross sections for Problem 2.

Table 3.7 shows the reaction rates over a region, $\int \sigma_t \phi \, dV$, for regions III and IV. The region IV is at the end of the duct.

For region III, the DSN method works well except the S_4 approximation. However, for region IV, even the S_8 approximation has a significant error. In comparison, the DCS and DCL methods give tolerable solutions for the DC_8 approximation in addition to their superiority over all orders of the DSN method. For this problem, the DCL method leads to more accurate solutions than the DCS method. This superiority, however, is compensated by the fact that the DCL method needs more memory and computing time.

PROBLEM 3

The preceding two problems show the ray effect mitigation by the DCN methods. To see their numerical properties, we solve a problem which has an analytical solution for the scalar flux. The geometry is illustrated in Fig. 3.6. The whole region is a vacuum except for an isotropic source region at the center, where the solution is obtained by the DSN method.

The analytical solutions are obtained by integrating the expression for the scalar flux at point $\underline{r}$ for a point source at $\underline{r}_0$ over the source region. A point source produces the following flux:

$$\phi_{pt} = \frac{S(\underline{r}_0)}{4\pi|\underline{r} - \underline{r}_0|} . \tag{3.18}$$

The result is

Table 3.7. Comparison of Region Reaction Rates for Problem 2

REGION/Method		III	IV
S_N	S-4	0.1745 (+8.3%)	0.05823 (-30.5%)
	S-6	0.1631 (+1.2%)	0.06899 (-17.6%)
	S-8	0.1599 (-0.76%)	0.07674 (-8.39%)
	S-16	0.1598 (-0.83%)	0.08594 (+2.59%)
DCS	DC-4	0.1683 (+4.5%)	0.06633 (-20.8%)
	DC-6	0.1619 (-0.50%)	0.07730 (-7.70%)
	DC-8	0.1600 (-0.70%)	0.08290 (-1.04%)
DCL	DC-4	0.1678 (+4.2%)	0.07209 (-13.9%)
	DC-6	0.1620 (+0.56%)	0.07954 (-5.05%)
	DC-8	0.1600 (-0.70%)	0.08364 (-0.153%)
MORSE		0.1611 (±3.18%)	0.08377 (±2.43%)

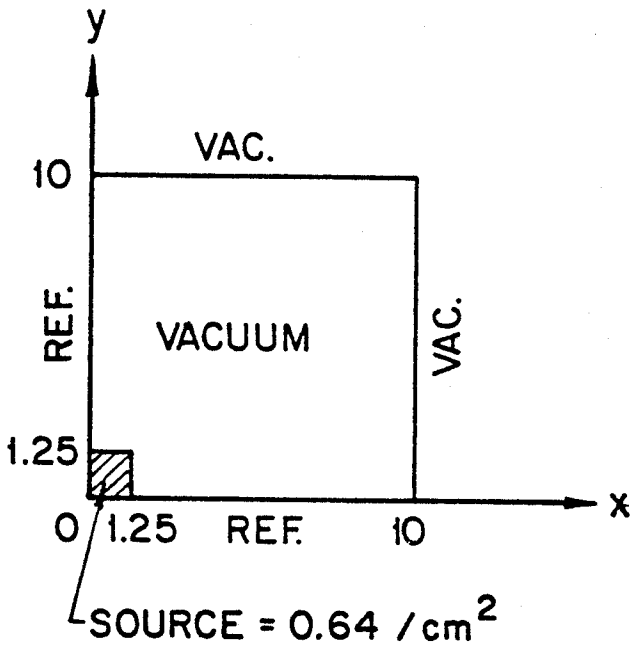

Fig. 3.6. Geometry for Problem 3.

$$\phi(x,y) = \frac{S}{4}\left\{\left|x - \frac{a}{2}\right| \ln \left|\frac{\frac{y - a/2}{x - a/2} + \left(\left(\frac{y - a/2}{x - a/2}\right)^2 + 1\right)^{1/2}}{\frac{y + a/2}{x - a/2} + \left(\left(\frac{y + a/2}{x - a/2}\right)^2 + 1\right)^{1/2}}\right|\right.$$

$$+ \left(x + \frac{a}{2}\right) \ln \left|\frac{y + \frac{a}{2} + \left(\left(x + \frac{a}{2}\right)^2 + \left(y + \frac{a}{2}\right)^2\right)^{1/2}}{y - \frac{a}{2} + \left(\left(x + \frac{a}{2}\right)^2 + \left(y + \frac{a}{2}\right)^2\right)^{1/2}}\right| \qquad (3.19)$$

$$+ \left|y - \frac{a}{2}\right| \ln \left|\frac{\frac{x - a/2}{y - a/2} + \left(\left(\frac{x - a/2}{y - a/2}\right)^2 + 1\right)^{1/2}}{\frac{x + a/2}{y - a/2} + \left(\left(\frac{x + a/2}{y - a/2}\right)^2 + 1\right)^{1/2}}\right|$$

$$\left. + \left(y + \frac{a}{2}\right) \ln \left|\frac{y + \frac{a}{2} + \left(\left(x + \frac{a}{2}\right)^2 + \left(y + \frac{a}{2}\right)^2\right)^{1/2}}{x - \frac{a}{2} + \left(\left(x - \frac{a}{2}\right)^2 + \left(y + \frac{a}{2}\right)^2\right)^{1/2}}\right|\right\}$$

where S is the source strength (neutrons/cm^3/second) and a is 2.5 cm for the present problem.

To estimate errors of the numerical solutions, the following L_2 error is calculated:

$$E_2 = \left[\sum_{i,j} \left\{1 - \frac{\phi_{ij}}{\phi(x_i,y_j)}\right\}^2 \Delta x_i \Delta y_j\right]^{1/2} \qquad (3.20)$$

where $\phi(x_i,y_j)$ is the analytical solution of scalar flux at a point (x_i,y_j), ϕ_{ij} is the solution by numerical method, and Δx_i, Δy_j are side lengths of a mesh cell. This special error norm is chosen because we are interested in the relative error to the analytical solution for the whole region.

The L_2 error, E_2, is presented in Table 3.8 for the DSN and DCN solutions. The problem is solved, varying the order of angle discretization, S_4, S_8, S_{16}, DC_4, DC_8, DC_{16} and the number of meshes, 8 × 8, 16 × 16, 32 × 32.

Table 3.8. Comparison of Relative Error of Scalar Flux for Problem 3

	8 x 8	16 x 16	32 x 32
DS_4	11.756	12.795	13.045
DC_4	5.466	6.2912	7.5012
DS_8	7.9132	8.0703	8.1624
DC_8	3.8341	4.065	4.8206
DS_{16}	4.727	4.3610	4.3569
DC_{16}	2.9669	2.5905	2.8082

In each box, the upper column is for the DSN solution, and the lower is for the DCS solution. The error for the DCS solutions is half as much as that for the DSN solutions. It is observed that refining the spatial mesh has less effect on the accuracy for both DSN and DCS solutions. Furthermore, refining the angle variables has less effect for the DCS method, compared with the DSN method. In regard to the spatial mesh refinement, the refinement indeed leads to better accuracy if standard L_2 error is observed; but, the effect is still small. The property of the DCS solution with respect to angle refinement suggests that the errors for the DSN and DCS solutions are closing as the order of angle discretization increases. In other words, the DCS approximation is especially useful for low order approximation.

PROBLEM 4

As an example of more realistic calculations by the discrete cones method, we solve a neutron transport problem of a conceptual fusion reactor. The geometry of the problem is illustrated in Fig. 3.7. This is a very simplified model of a cross section of a tokamak reactor with a bean shape plasma. The spatial domain is partitioned uniformly into 27 times 15 mesh cells. The outer structure is made of a tungsten shield. The problem is solved by TWODCXY (DSC_8-P_3) and TWOTRAN-II (S_8-P_3) by using 30 neutron and 12 gamma energy groups. Here DSC_N implies that the S_N approximation and the DC_N approximation are used in a non-void and a void, respectively. The neutron and gamma cross section data are taken from a public cross section library XSLIB5 available at the National Magnetic Fusion Engineering Computer Center (NMFECC).

Source neutrons are distributed uniformly over the second energy group, which ranges from 13.5 MeV to 15 MeV. The input source distribution is shown

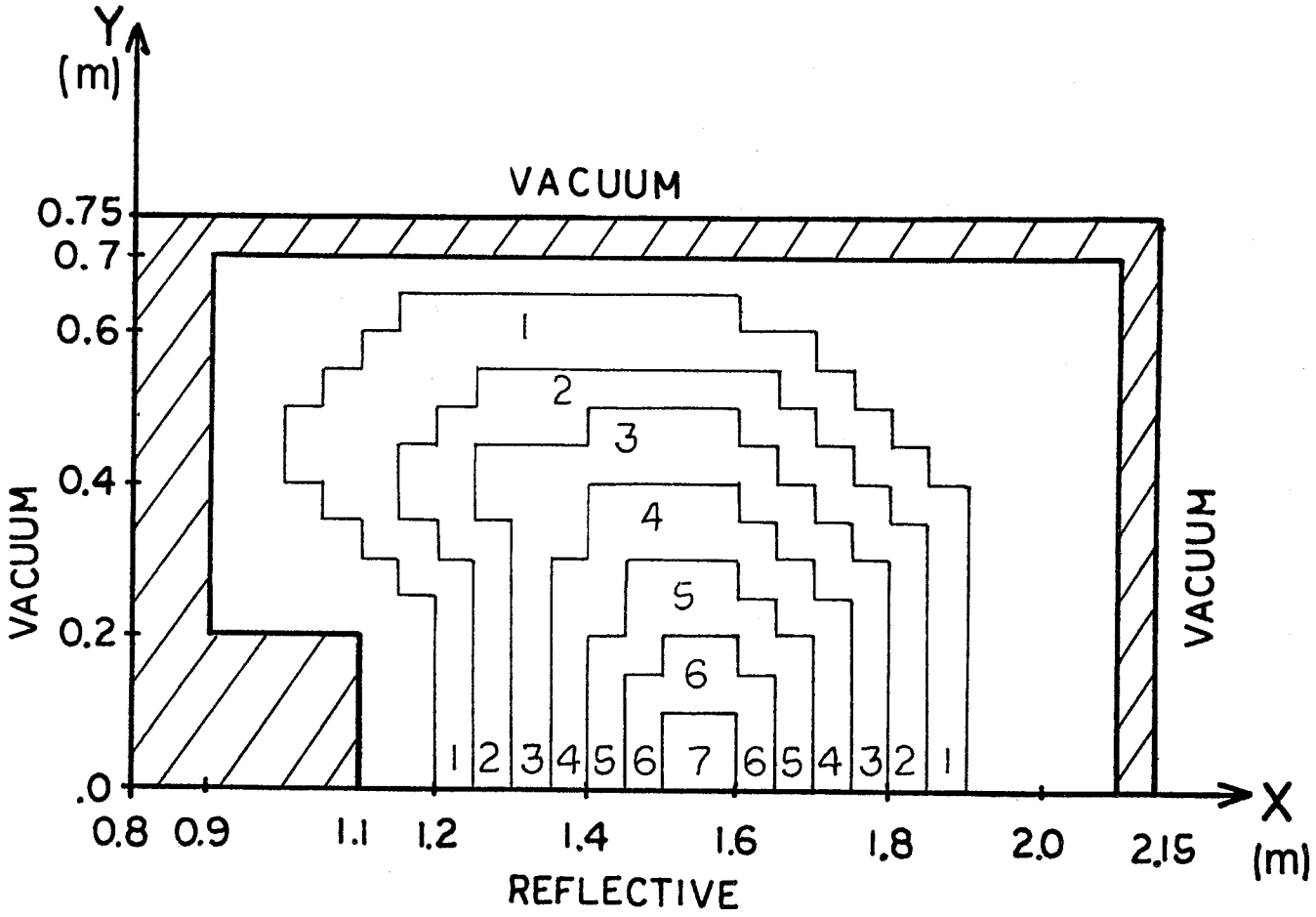

Fig. 3.7. Geometry of Problem 4.

in Fig. 3.7, where the numbers denote relative intensity of the source. Actual solutions are obtained by setting the total source to unity.

Figures 3.8 and 3.9 show the scalar flux of the second energy group. In Figs. 3.8(a) and (b), the contours of the flux distribution are plotted for the S_8 and DSC_8 solutions, respectively. The only difference between the two solutions is that, since the ray streaming effects are mitigated, the contours of the DSC_8 solution are smoother than those of the S_8 solution. The scalar flux distributions along outer edges of the system are shown in Fig. 3.9(a), (b), and (c) for X = 0.825, y = 0.725, and x = 2.125, respectively. Fig. 3.9(a) shows the DSC_8 method eliminates the ray streaming effect.

The CPU times of the two calculations are 197.9 seconds for the DSC_8 calculation and 189.3 seconds for the S_8 calculation.

In conclusion, the new program TWODCXY is better than the TWOTRAN program in practical situations as well as in simple one-energy group calculations.

References for Section 3

1. K.D. Lathrop and F.W. Brinkley, "TWOTRAN-II: An Interfaced, Exportable Version of the TWOTRAN Code for Two-Dimensional Transport," Los Alamos Scientific Lab., LA-4848-MS (1973).

2. M.B. Emmett, "The MORSE Monte Carlo Radiation Transport Code System," Oak Ridge National Lab., ORNL-4972 (1975).

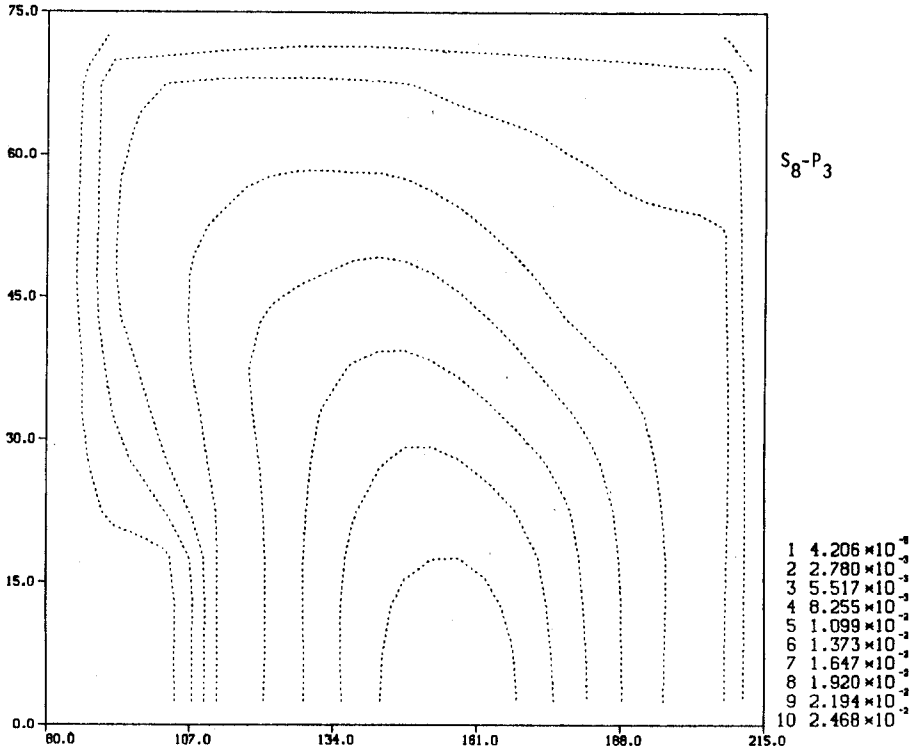

(a)

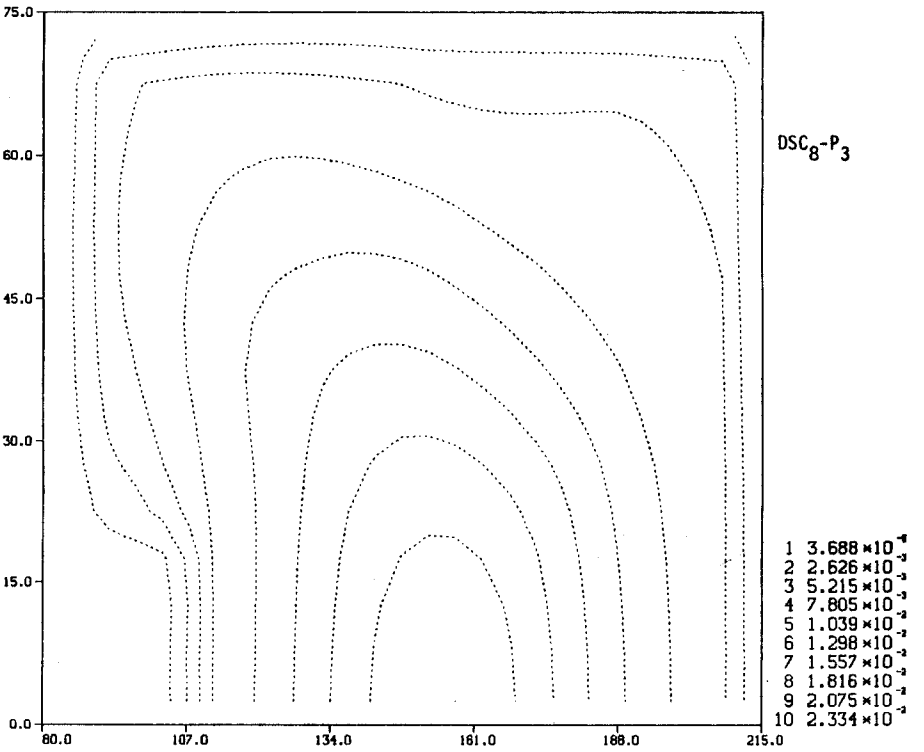

(b)

Fig. 3.8. (a) A contour plotting of scalar flux, S_8P_3.
(b) A contour plotting of scalar flux, DSC_8-P_3.

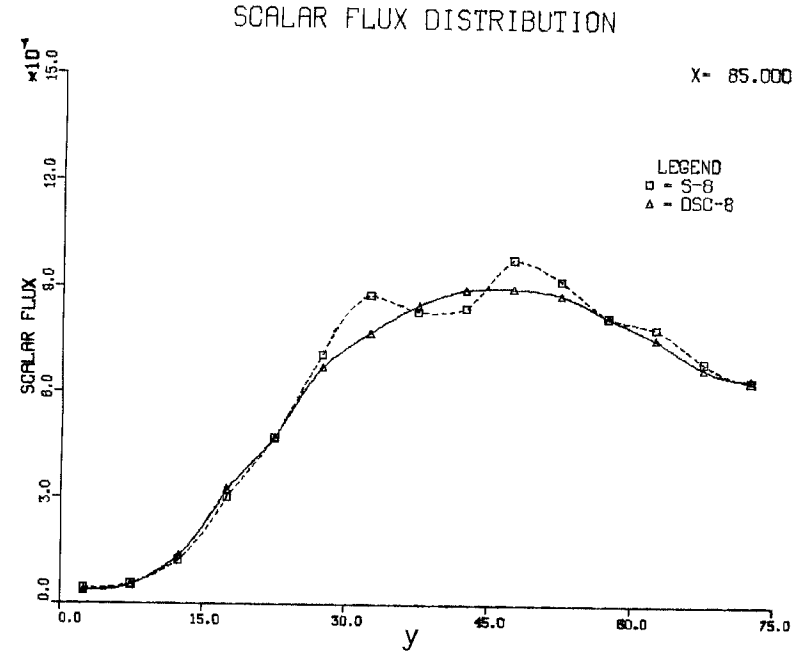

Figure 3.9

(a) Scalar flux at x=85 cm.

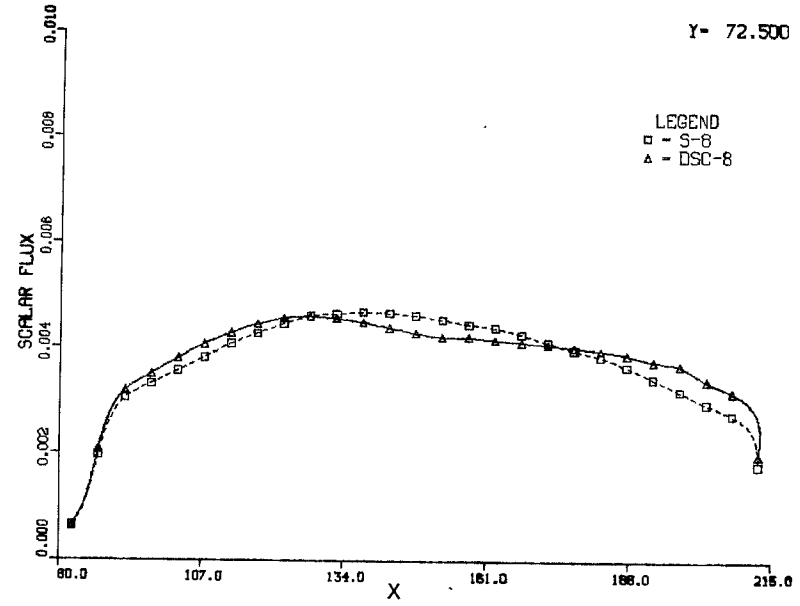

(b) Scalar flux at y=72.5 cm.

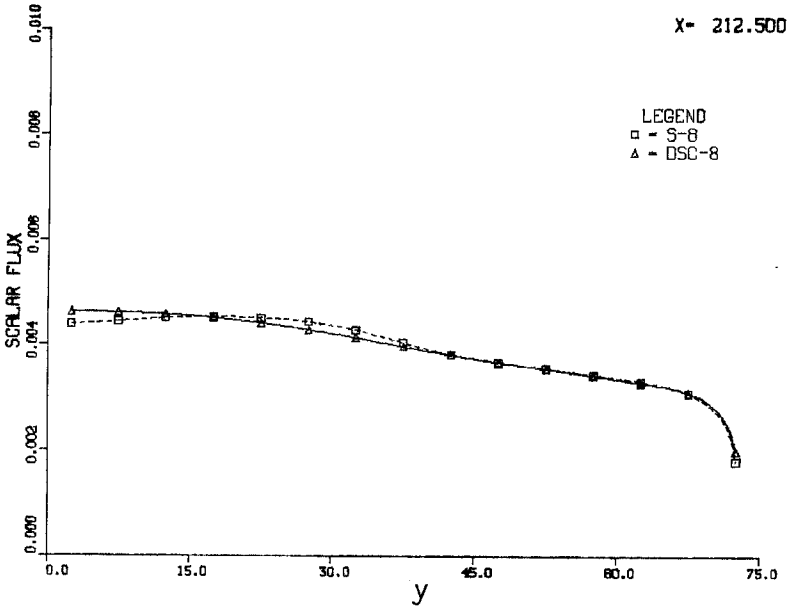

(c) Scalar flux at x=212.5 cm.

4. CONCLUSIONS

A theory of the discrete cones method was developed, and the new method was applied to a solution in a void for X-Y geometry. By utilizing the new computational schemes for a void region in a standard discrete ordinates, hybrid programs were created and tested.

Sample problems demonstrate strong mitigations of the ray streaming effect for low order approximations of angle discretization. We also found that the discrete cones method applied to a void mesh cell (the DCS program) is more efficient in terms of computing time and needs less computer memory than the discrete cones method formulated for subsurfaces of void boundaries (the DCL program).

Hence, the DCS scheme was implemented in the TWOTRAN-II program to create a new program TWODCXY, which is almost identical to the original program from user's point of view except some additional inputs about voids. The TWODCXY program was used to solve a realistic multigroup problem encountered in a fusion reactor study. It was shown that the new program results in a more accurate solution than TWOTRAN-II without any penalty of computing cost.

The current discrete cones approximations were formulated under three assumptions:

1. an angular flux is constant over a cone;
2. a cell-edge angular flux is constant over a boundary surface of a mesh cell or a boundary subsurface of a void; and
3. a particle source is constant in a void cell.

Because of the first assumption, the ray streaming effect is not completely mitigated. To obtain better accuracy, we adopted a linear approximation. The scheme results in better solutions than the constant approximation for some

problems, but the solutions display erroneous behaviors in some cases.[1] Meanwhile, applying linear or higher order approximation to spatial variables enables us to use coarser void mesh cells.

From the practical point of view, the discrete cones method must be applied to R-Z geometry. Since the linear approximations described in the above paragraph cannot be formulated in R-Z geometry without considerable effort, we shall apply the constant approximation, which will be reported in a forthcoming paper. Also, the method will be applied to a solution in non-vacuum media with an anticipation of the ray effect mitigation.

References for Section 4

1. Y. Watanabe, "Preliminary Report," October 1982, (not published).

Acknowledgment

The authors would like to thank Dr. T. Seed at INESCO Company for providing his program, STRMEX. The authors also wish to thank Dr. F.W. Brinkley for providing the TWOTRAN-II program. The work was supported by the Department of Energy.